Journal of Hydrology: Regional Studies 60 (2025) 102498

Contents lists available at ScienceDirect

Journal of Hydrology: Regional Studies

journal homepage: www.elsevier.com/locate/ejrh

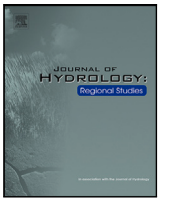

Uneven shifts in flood and drought flows in a Brazilian water supply catchment

Tiago Souza Mattos [a], André Simões Ballarin [b], Murilo Cesar Lucas [c,*], André Almagro [a], Paulo Tarso Sanches Oliveira [a]

[a] Faculty of Engineering, Architecture and Urbanism and Geography at Federal University of Mato Grosso do Sul, Costa e Silva Av, Campo Grande, 79070900, Mato Grosso do Sul, Brazil

[b] Department of Hydraulics and Sanitary Engineering, São Carlos School of Engineering, University of São Paulo, 400 Trabalhador são-carlense Avenue, São Carlos, 13566590, São Paulo, Brazil

[c] Universidade Estadual de Campinas, 1888 Pachoal Marmo St, Limeira, 13484050, São Paulo, Brazil

ARTICLE INFO

Dataset link: https://doi.org/10.7910/DVN/1C9NV2, Uneven shifts in flood and drought flows in a Brazilian water supply catchment - Dataset (Original data)

Keywords:
Global warming
Hydrological extremes
Water resources
Water scarcity

ABSTRACT

Study Region: Passaúna catchment, Paraná State, Brazil.

Study Focus: This study assessed the impacts of projected climate change on streamflow (Q) regimes and dynamics in the study area, a key drinking water source for the Curitiba Metropolitan Region (3.7 million people). Dry and wet Q regimes were analyzed using 3-, 6-, and 12-month accumulation periods through a non-parametric approach. Changes in Q extremes — drought and flood flows — were evaluated using a frequency-based method. Daily Q was simulated by a Long Short-Term Memory (LSTM) network and the lumped conceptual Hydrological Model 2 (HyMod2), both forced with bias-corrected CMIP6 historical (1980–2013) and future (2015–2100) climate scenarios.

New Hydrological Insights: Agreement was observed between hydrological models (KGE = 0.83; NSE = 0.79), though both showed limitations in simulating extreme flows. Projections indicate no statistically significant changes in drought flow duration and severity across future scenarios. In contrast, wet regimes are expected to intensify, with durations increasing by up to two months in the mid and far future under SSP5-8.5. Flood flows show a consistent positive trend, with the 100-year event projected to increase by 26% under SSP2-4.5 and 52% under SSP5-8.5. Findings suggest a shift toward wetter conditions and more frequent floods, highlighting the importance of considering adaptive reservoir operation and resilient infrastructure planning in the Passaúna catchment.

1. Introduction

Since a part of the scientific community has recognized that the stationarity of hydrometeorological processes is no longer valid (Milly et al., 2008; Bartiko et al., 2017; Foufoula-Georgiou et al., 2015), projecting future streamflow regimes becomes crucial for water resource management. In a global warming context, concerns over the adverse impacts of climate change drive scientific efforts to illuminate how the nonstationarity of streamflow will affect water availability and demand. The imbalance between these factors leads to water scarcity (Van Loon and Van Lanen, 2013). Ensuring access to drinking water is a key objective of the United

* Corresponding author.
E-mail address: mlucas@unicamp.br (M.C. Lucas).

https://doi.org/10.1016/j.ejrh.2025.102498
Received 12 February 2025; Received in revised form 12 May 2025; Accepted 30 May 2025
Available online 25 June 2025

Nations' Sustainable Development Goals (SDGs) in the 2030 Agenda (United Nations, 2015). Hence, underscoring comprehensive assessments of streamflow regimes under climate change is vital in the role of water availability (Gudmundsson et al., 2021).

While studies argue that the hydrological cycle is not intensifying (Koutsoyiannis, 2020), others demonstrate that changes are expected for the future (Ficklin et al., 2022; Wang et al., 2023) due to climate change by altering the rate of water fluxes to and from the terrestrial surface. For instance, in regions of Brazil (Chagas et al., 2022), the United States (Brunner et al., 2020), and China (Liu et al., 2024), climate change is expected to drive significant shifts in future streamflow regimes, contributing to more frequent and severe extremes, such as droughts and floods. Some studies indicate that the likelihood of severe precipitation events is increasing, disrupting streamflow patterns and elevating flood risks (e.g., Tabari, 2020; Asadieh and Krakauer, 2017). In Brazil, 100-year precipitation events are projected to intensify by 17% under moderate climate change scenarios and by 31% under the most extreme projections (Ballarin et al., 2024b). Furthermore, the transition between drought and flood events is expected to occur more abruptly, amplifying hydrological variability and its associated challenges (Rezvani et al., 2023).

Besides flood risk, intensified droughts induced by climate change are a major concern. Droughts put pressure on ecosystems (Zhang et al., 2021), water and food supplies (Scanlon et al., 2023), hydroelectric production, and tourism. Globally, droughts have exhibited a trend of intensifying conditions and are projected to increase in frequency and intensity in the future (Wang et al., 2021). Southwestern South America, Mediterranean Europe, and Northern Africa may experience unprecedented hydrological drought conditions within the next 30 years under a climate change scenario (Satoh et al., 2022). In Brazil, projections indicate an increase in meteorological drought frequency and severity, driven by higher evapotranspiration rates, fewer wet days, and reduced precipitation exceeding evaporation (Ballarin et al., 2024a).

Recurrent droughts have led to water crises in some Brazilian megacities, where millions of people rely on surface water reservoirs. These droughts have resulted in social unrest and economic losses in metropolitan areas that depend heavily on surface water reservoirs. For instance, the São Paulo Metropolitan Region (SPMR) nearly ran out of water in 2015 due to a severe meteorological drought and antecedent soil moisture conditions (Melo et al., 2016). Gesualdo et al. (2019) showed increasing levels of water insecurity for the SPMR toward the 21st century under climate change scenarios. Similarly, another severe meteorological drought triggered water scarcity in the Curitiba Metropolitan Region (CMR). The Curitiba Metropolitan Region (CMR) avoided running dry due to water use restrictions implemented by the Paraná Sanitation Company (SANEPAR) between March 2020 and January 2022.

While broader-scale global assessments offer valuable insights, a critical gap remains in understanding the specific impacts of climate change on the hydrological regimes of individual catchments, especially those vital for urban water supply. Here, the objective is to bridge this gap by assessing the projected changes in hydrological dynamics and regimes in the Passaúna catchment, a vital drinking water source for the CRM. This catchment supplies fresh water to 690,000 inhabitants and has already experienced severe droughts in recent years.

The research questions addressed here are as follows: (1) How is climate change expected to impact the long-term mean streamflow wet and dry regimes in the Passaúna catchment over the 21st century? (2) What are the projected changes in hydrological extremes (floods and droughts) under different climate scenarios? (3) How will these changes affect water and catchment management? Answering these questions offers valuable insights to support water managers in adapting to projected future scenarios.

2. Study area

The Passaúna catchment was selected as the study area (Fig. 1) because it supplies fresh water to the CMR. This catchment is a critical water source and has experienced severe hydrological droughts recently, facing water scarcity. We are concerned about whether projected climate change will intensify such droughts in the future. While other megacities in Brazil, such as the SPMR (~21 million people), may also be of interest, this is the first study to address the impacts of climate change on the drinking water source of the CMR. The Passaúna catchment, covering 218 km^2 with an average elevation of 942 m a.m.s.l, comprises the municipalities of Curitiba, Araucária, Campo Largo, Campo Magro, and Almirante Tamandaré in Paraná State, southeastern Brazil.

The Passaúna River is regulated by the Passaúna Dam upstream. The water reservoir has a surface area of 895 ha and a current volume of 69.3 hm^3, with the spillway level at 887.2 m a.m.s.l (Hilgert et al., 2019). The Passaúna reservoir supplies water to nearly 690,000 people. The CMR Water Supply System includes the Iguaçu system (3.3 m^3/s), the Iraí reservoir (2.6 m^3/s), the Passaúna reservoir (1.8 m^3/s), and the Miringuava reservoir (0.9 m^3/s).

The annual mean rainfall ± standard deviation between 1979 and 2010 was 1456 ± 239 mm, with minimum and maximum values of 916 and 1944 mm/year, respectively. The average minimum temperatures range between 12 and 13 °C, while the maximum temperatures range between 22 and 23 °C. According to Köppen's climate classification, the climate is temperate oceanic or humid mesothermal (Cfb) (Alvares et al., 2013).

Land use and land cover are dominated by agriculture and pasture (48%, mostly agriculture), followed by native forest (32%), non-vegetated areas (15%, mostly urban areas), surface water (4%), and non-native forest (1%). Since 1985, urban areas have expanded significantly in the southern catchment, particularly towards the downstream reservoir and around the western inlet of the Passaúna River reservoir.

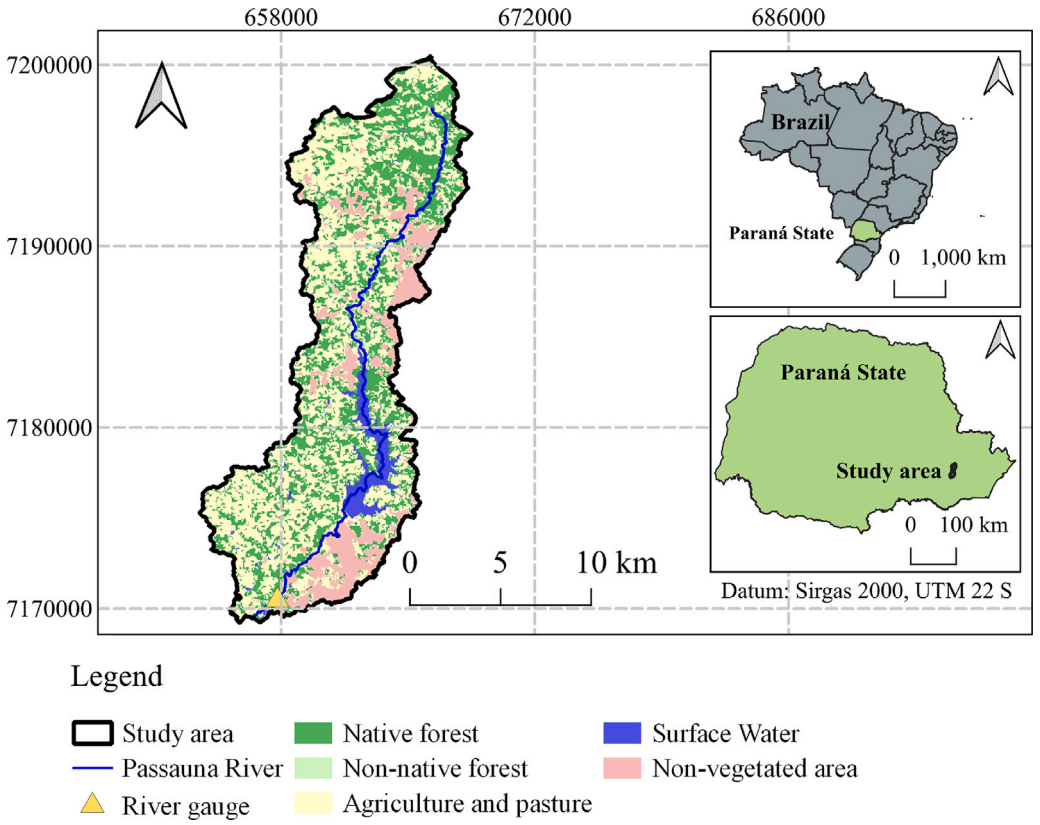

Fig. 1. Location of the study area, land use and land cover for the year 2021, and river gauge. Land use and land cover data were obtained from the MapBiomas Project — Collection 7.0 (Mapbiomas, 2023). The study area was delineated using the Copernicus Digital Elevation Model at 30-m resolution.

3. Data sources

3.1. Measured datasets

Quantitative daily datasets of precipitation (P), potential evapotranspiration (PET), and streamflow discharge (Q) from ten catchments were used over the 1986–2010 period (Table 1). The location of the ten catchments is presented in Figure S1. Furthermore, several static attributes of these catchments were also used as follows: catchment mean slope, percentage covered by broad-leaved or needle-leaved forests, percentage covered by grasslands or areas with sparse (<15%) vegetation, percentage covered by artificial surfaces or urban areas, subsurface porosity and permeability of the catchment, and percentage of soil texture (sand, silt, and clay).

It is important to note that the observed quantitative and static attributes of ten catchments, including the study area, were used to train and test a Long Short-Term Memory (LSTM) model, while only quantitative data from the Passaúna catchment were used to calibrate and validate a conceptual hydrological model.

The datasets came from the Catchment Attributes and Meteorology for Large-sample Studies — Brazil (CAMELS-BR), which provides hydrometeorological and static data for hundreds of Brazilian catchments (Chagas et al., 2020). Daily PET data were derived from the Global Land Evaporation Amsterdam Model (GLEAM), version 3.3a, at a 0.25° × 0.25° spatial resolution (Martens et al., 2017). Daily P data were sourced from the Multi-Source Weighted-Ensemble Precipitation (MSWEP), version 2.2, available within CAMELS-BR (Beck et al., 2019). Daily streamflow (Q) data were obtained from the Brazilian National Water and Sanitation Agency (ANA), with the Passaúna catchment corresponding to river gauge station code 65024000.

3.2. Climate change dataset

A bias-corrected CLIMate change dataset for Brazil (CLIMBra) was used as input in trained (or calibrated) hydrological models to predict changes in future Q regimes over the 2015–2100 period (Table 1). CLIMBra provides gridded data at a 0.25° × 0.25° resolution and includes six bias-corrected climate variables (precipitation, maximum and minimum air temperature, solar radiation, near-surface wind speed, and relative humidity) derived from ten different General Circulation and Earth System Models (GCMs/ESMs): MRI-ESM2, EC-EARTH3, CMCC-ESM2, INM-CM4-8, NorESM2-MM, MPI-ESM1.2-HR, INM-CM5, ACCESS-ESM1-5,

Table 1
Summary of the observed and projected climate change datasets.

Dataset	Source	Spatial resolution	Period
Daily Precipitation (P)	MSWEP (CAMELS-BR) (Beck et al., 2019)	0.25° × 0.25°	1986–2010
Potential Evapotranspiration (PET)	GLEAM v3.3a (CAMELS-BR) (Martens et al., 2017)	0.25° × 0.25°	1986–2010
Streamflow (Q)	National Water and Sanitation Agency (ANA)	–	1986–2010
Static attributes	CAMELS-BR (Chagas et al., 2020)	–	–
Climate Projections (SSP2-4.5 and SSP5-8.5)	CLIMBra (Bias-Corrected CMIP6 GCMs/ESMs) (Ballarin et al., 2023b; Cannon et al., 2015; O'Neill et al., 2016)	0.25° × 0.25°	1980–2013 (historical period) and 2015–2100 (future period)
General Circulation Models (GCMs/ESMs)	MRI-ESM2, EC-EARTH3, CMCC-ESM2, INM-CM4-8, etc (CMIP6)	0.25° × 0.25°	2015–2100

IPSL-CM6 A, and MIROC6. The models' simulations were developed under the Coupled Model Intercomparison Project Phase 6 (CMIP6) context and were selected based on the availability of the variables required to run the hydrological simulations. The entire year of 2015 was excluded from the projected future simulation because the LSTM input sequences used a time step of 270 days, and the conceptual hydrological model a warm-up period of 360 days.

CLIMBra's bias correction was performed using the Quantile Delta Mapping (QDM) method (Ballarin et al., 2023b; Cannon et al., 2015), using a Brazilian gridded dataset (i.e., Xavier et al., 2016). Here, two Shared Socioeconomic Pathways (SSPs) were considered (O'Neill et al., 2016): (1) the middle-of-the-road scenario (SSP2-4.5) and (2) the fossil-fueled development scenario (SSP5-8.5). The impacts of these scenarios were analyzed across three time frames: the immediate future (2015–2040), the mid-century future (2041–2070), and the late-century future (2071–2100).

SSPs enhance the utility of Global Climate Models (GCMs) by outlining a range of possible future socioeconomic developments. These scenarios help researchers explore how human activities might influence greenhouse gas emissions and the global climate system. Together, GCMs and SSPs are an integrated framework that supports an understanding of potential climate futures and aids policymakers in evaluating the likely consequences of climate change across different sectors (Anwar et al., 2024).

4. Methods

An overview of the methodological framework adopted in this study is presented in Fig. 2. Initially, the observed datasets (Table 1) were used to calibrate and train two types of hydrological models, respectively: a theory-driven and a data-driven model. Once calibrated and trained, both models were forced with climate change projections of P and PET derived from the CLIMBra dataset. The resulting Q simulations under historical and future climate scenarios were analyzed to characterize wet and dry regimes, flood and drought flows.

The performance of the conceptual hydrological model during the validation period was compared to that of the LSTM during the test period to assess whether the choice between a theory-driven and a data-driven modeling approach affects the results related to Q dynamics and regimes. This comparison was designed to test the hypothesis that the consistency of findings may not depend on the underlying hydrological model structure. It was further hypothesized that structural differences between the models would not constitute the dominant source of uncertainty in the simulations. The comparison was solely evaluated for the Passaúna catchment.

4.1. Conceptual hydrological model

The Hydrological Model 2, HyMod2 (Roy et al., 2017) — an updated version of the HyMod (Boyle, 2001; Wagener et al., 2001), a lumped, parsimonious, conceptual rainfall-runoff model — was selected as the benchmark hydrological model to simulate Q. The key difference between the two models lies in the structural modifications related to the parameterization of the evapotranspiration process. The model is driven using daily P and PET data to generate estimates of actual evapotranspiration (Roy et al., 2017).

HyMod2 consists of two main components: the excess rainfall (runoff generation) component and the routing (runoff routing) component. The excess rainfall component estimates runoff based on soil moisture storage using a saturation-excess mechanism. Spatial variability in catchment soil storage capacity is represented by a Pareto distribution, characterized by the maximum soil moisture storage capacity, $C_{\max}$ (in units of mm). $C_{\max}$ is calculated based on the maximum indicator height (H_{max}) and a dimensionless shape parameter (b), which describes the heterogeneity of soil moisture capacity across the catchment.

The resulting excess rainfall is then partitioned into quick- and slow-flow via the α parameter. The routing module routes each pathway through linear reservoir cascades: a series of identical reservoirs (N_q) for quick-flow (or surface runoff), each of one governed by the routing coefficient (k_q), and a single reservoir for slow-flow (or baseflow), governed by the routing coefficient (k_s). These two flow components are then summed to produce the Q at the catchment outlet. Finally, HyMod2 accounts for an Evapotranspiration-Resistance (ER) term for the soil moisture. There are three parameters to describe ER: the maximum ER

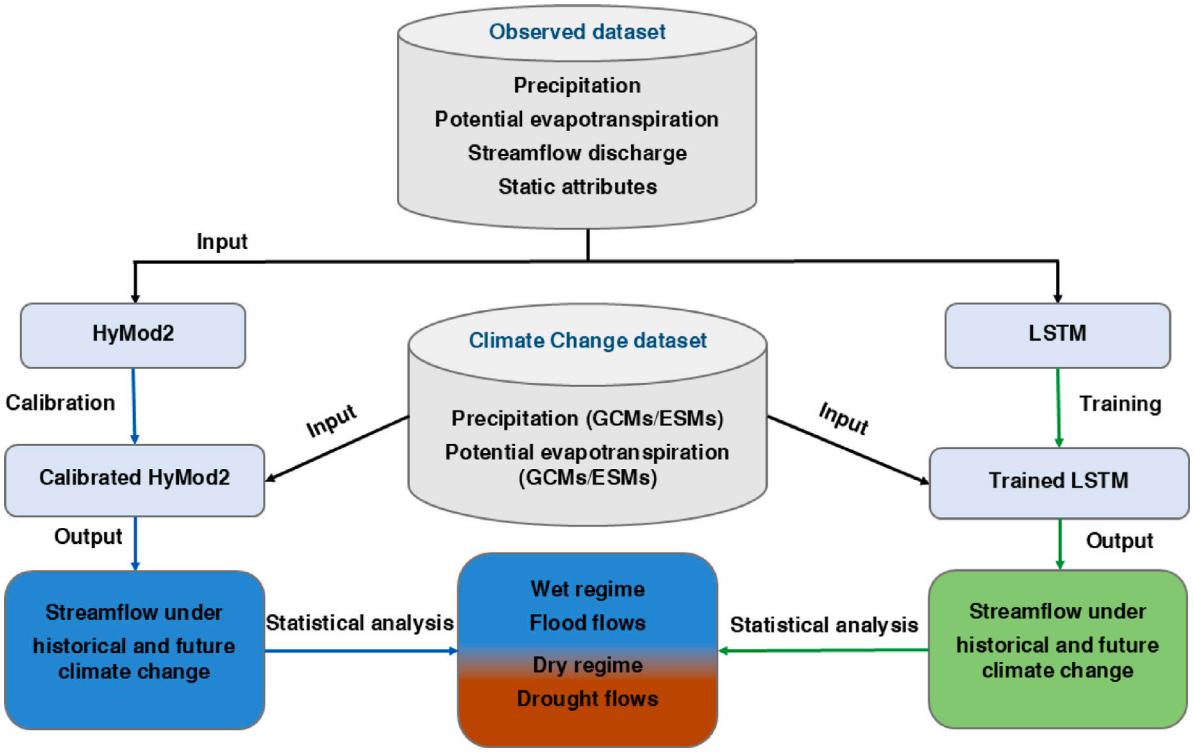

Fig. 2. Overview of the research protocol.

factor (K_{max}), the fractional multiplier defining the lower resistance (γ), and the exponent controlling the nonlinearity of the resistance-to-storage relationship (BE).

In summary, HyMod2 simulates Q using nine parameters: $H_{\max}$ and b for the excess rainfall component, α, k_s, and k_q for the routing component, and K_{max}, γ, and BE for ER. HyMod2 may be considered a simple yet effective model because: (1) it requires only a small number of parameters; (2) it does not depend on topographic or land use data; and (3) it is driven solely by P and PET.

The original HyMod (Boyle, 2001) has been used in the Brazilian territory. For instance, to reproduce the hydrology at the basin scale and analyze the outcomes of reservoir expansion in terms of water security (Meira Neto et al., 2024). Furthermore, to assess the impact of climate change on water security of the Cantareira Water Supply System (Gesualdo et al., 2019) in the SPMR. Satgé et al. (2021) evaluated the performance of the ECMWF-SEAS5 global precipitation product for predicting Q regimes in a tropical river basin in Brazil.

4.2. Data-driven deep learning model

Artificial Neural Networks (ANNs) originated within the field of Artificial Intelligence (AI), based on the idea that computational models inspired by the structure of the human brain could learn and improve through experience. ANNs serve as the foundational architecture for various specialized neural network types, including Recurrent Neural Networks (RNNs). RNNs extend traditional ANNs by incorporating recurrent connections that allow information to persist across sequences, making them suitable for time-dependent data. However, standard RNNs often struggle to learn long-term dependencies due to issues like vanishing and exploding gradients. To overcome these challenges, Long Short-Term Memory (LSTMs) networks were developed as an advanced form of RNN. LSTMs incorporate gating mechanisms that control the flow of information and enable the model to retain relevant data over longer sequences (Hochreiter and Schmidhuber, 1997; Kratzert et al., 2019a).

An LSTM unit comprises a memory cell and a set of control gates—namely, input, forget, and output gates. The memory cell maintains information over time through weighted activation functions, while the gates regulate the flow of information into, within, and out of the cell. These gates determine which information should be retained, updated, or discarded at each time step. The main components of an LSTM network include: (a) the hidden state, which influences decisions on memory updates; (b) the input state, formed by combining the hidden state and current input; (c) the cell (internal) state, responsible for carrying long-term information; (d) the input gate, which governs how much new information is stored; (e) the forget gate, which decides which past information to discard; and (f) the output gate, which determines the information passed to the next hidden state and output layer. For a more detailed description, see Kratzert et al. (2018).

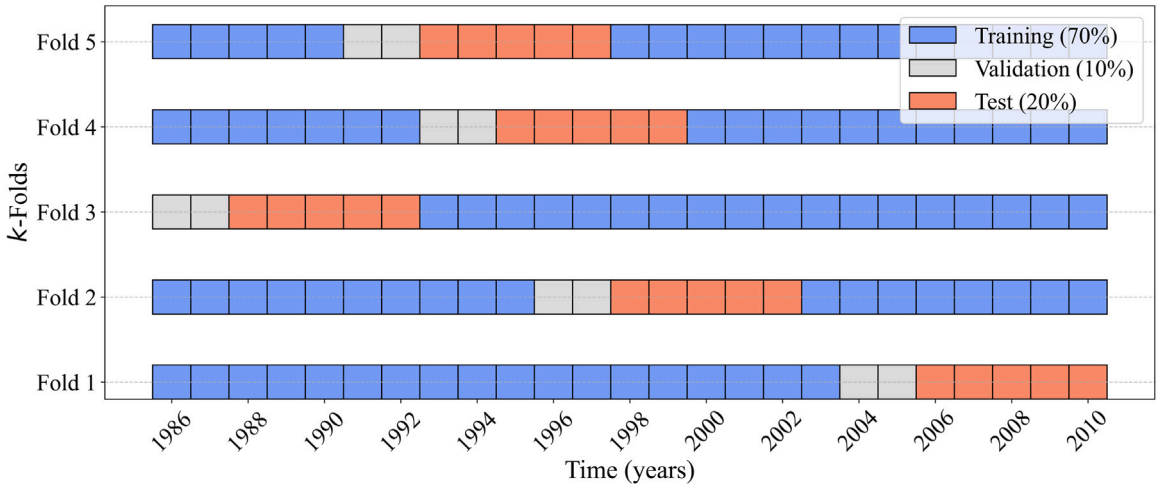

Fig. 3. Representation of the five k-fold cross-validation strategy for hydrological simulation using LSTM model.

Here, an LSTM algorithm was selected for simulating Q at the Passaúna catchment. The LSTM came from the NeuralHydrology API (Kratzert et al., 2018), which applies LSTMs as a generalized rainfall-runoff model. LSTM network stands out as a good choice for hydrological modeling, particularly for simulating catchment processes such as rainfall-runoff transformation. LSTMs have been successfully applied in numerous hydrological studies, demonstrating their robustness and reliability across diverse catchments and climatic conditions (Kratzert et al., 2018, 2019a; Xu et al., 2023; Wang et al., 2024).

First, LSTM model was trained using observed P, PET, Q, and static attributes (Table 1) of the ten catchments (Fig. S1). Including static attributes enhances the model's ability to capture the underlying dynamics of the time series data by providing essential contextual information (Kratzert et al., 2019b). LSTM model was trained using data from all ten catchments; that is, one set of parameters was optimized to generalize across the ten catchments. Training a single LSTM model on multiple catchments offers several advantages: (1) it enhances generalization by exposing the model to diverse hydrological conditions; (2) allows it to learn from a larger dataset; and (3) leverages shared patterns across catchments to improve predictive accuracy (Kratzert et al., 2024). Finally, the trained LSTM was run for the Passaúna catchment using the bias-corrected climate change as input to simulate historical and future periods.

4.2.1. LSTM hyper-parameters

Hyperparameters are crucial in designing and optimizing LSTMs, acting as tunable settings that dictate how a model learns from data. They define the model's structure, such as the number of hidden layers and the activation functions used, and significantly impact the efficiency and accuracy of model training (Yu and Zhu, 2020). The number of hidden/cell states, dropout rate, and length of the input sequence were determined by conducting a grid search over a range of parameter values. Specifically, the following parameter values were investigated: hidden states (64, 128, 192, and 256), dropout rate (0.0, 0.2, 0.4, and 0.5), and length of the input sequence (90, 180, 270, and 365 days).

Here, LSTM architecture consisted of 128 memory cells and a single fully connected layer with a dropout rate of 0.5. The LSTM was designed to predict daily Q values using meteorological forcing data from the previous 270 days and the forcing data of the target day. Additionally, a batch size of 256 samples was used with a learning rate of 1×10^{-4}, 100 training epochs, and the Mean Squared Error (MSE) as the loss function.

4.2.2. LSTM cross-validation strategy

Following Goodfellow et al. (2016), a training strategy for the LSTM was implemented by partitioning the data into three subsets: training, validation, and test datasets over the 1986–2010 period. The k-fold cross-validation strategy (varying k between 1 and 5) was used to partition the dataset for each catchment into training (70%), validation (10%), and test (20%) sets (Fig. 3).

For each of the five folds, LSTM was trained on a sequence of years, while a single year was designated for validation, and the remaining years were used for testing. This approach ensured that the model was trained on a diverse dataset while validating and testing its performance on separate, unseen data. By systematically shifting the training and validation periods across the folds, the robustness of LSTM evaluation were enhanced. The optimal k-fold configuration was selected based on the mean Kling–Gupta efficiency, KGE (Gupta et al., 2009), highest score considering the ten catchments during the test period.

4.3. Assessment of HyMod2 and LSTM performance

Evaluating hydrological model performance plays a critical role in the processes of calibrating and validating. The performance of the LSTM and HyMod2 models during the training (or calibration) and testing (or validation) periods was evaluated by comparing observed and simulated Q. No single indicator adequately captures model behavior across all flow dynamics. Hence, a set of five metrics was applied to hydrological model evaluation.

Models' performance was evaluated using a combination of error and efficiency metrics. Root Mean Squared Error ($RMSE$) was used to quantify the mean error. The Nash–Sutcliffe Efficiency, NSE (Nash and Sutcliffe, 1970), and the KGE were applied as goodness-of-fit measures to assess the agreement between observed and simulated Q. To evaluate models' performance under hydrological extremes, the percent bias for the top 2% of peak-flows (FHV) and the bottom 30% of low-flows (FLV) (Yilmaz et al., 2008) were used. These indicators reflect the models' skill to simulate extreme high- and low-flow regimes (referred to here as flood and drought flows, respectively). Positive values of FHV and FLV indicate overestimation, while negative values indicate underestimation.

4.4. Future dry and wet regimes

Hydrological dry and wet regimes were identified using the non-parametric approach proposed by Ukkola et al. (2020). This approach, which resembles the widely used Standardized Precipitation Index (SPI), introduced by Mckee et al. (1993) for meteorological droughts, does not require any prior assumptions regarding data distribution. The identification of drought regimes involves three core steps. First, daily Q series are accumulated into x-day running totals. In this study, $x = 3$, 6, and 12 months were used to capture hydrological variations over seasonal and annual scales, accounting for the soil moisture memory effect (Orth and Seneviratne, 2012). Second, the 15th percentile of the accumulated values is calculated separately for each calendar month during the historical baseline period (1980–2010). This percentile threshold is then used to identify drought events, defined as periods when the monthly accumulation falls below this reference value. The same approach was also applied to identify meteorological droughts by using P instead of Q.

The same procedure was applied to identify wet regimes, with wet events defined as months in which accumulated flows exceeded the 85th percentile threshold. The selected drought percentile approximately corresponds to a SPI value of -1, which is widely adopted for identifying drought conditions (Ukkola et al., 2020). The same principle is applied to wet regimes, where the 85th percentile approximates an SPI of $+1$. To ensure consistent comparison across time periods, the 15th and 85th percentiles calculated for the historical period (1980–2010) were used as fixed reference thresholds for identifying dry and wet regimes in both historical and future climate scenarios.

Following the definition proposed by Ballarin et al. (2024a), the duration of dry and wet regimes is defined as the period between the onset and cessation of a specific event. For instance, a dry regime event is characterized by consecutive months in which the 3-, 6-, or 12-month running accumulation series falls below the corresponding monthly 15th percentile. In contrast, wet regimes are defined using the 85th percentile threshold. The severity of each event is computed as the cumulative deviation of the running accumulation series from the respective threshold (i.e., the 15th or 85th percentile for dry and wet regimes, respectively).

4.5. Drought and flood flows

To further investigate potential changes in extreme hydrological regimes, namely drought and flood flows, the framework proposed by Chagas et al. (2022) was adopted. Specifically, annual series of the minimum 7-day streamflow ($Q7_{\min}$) and the maximum daily streamflow ($Q_{\max}$) were used to represent drought and flood flows, respectively. This approach complements the previous analysis of dry and wet regimes based on longer accumulation periods and soil moisture memory effects. By incorporating short-term extremes, the framework provides a more refined understanding of hydrological variability, which is particularly relevant for assessing rapid-onset events that critically affect water resources management, ecosystem resilience, and infrastructure vulnerability.

For drought flows, projected changes in $Q7_{\min}$ were computed between the historical period and the near-, mid-, and far-future periods, with assessments of both statistical significance and temporal trends. Projected changes in flood flows were analyzed using a frequency-based statistical approach. Following Zaghloul et al. (2020), two alternative statistical distributions — Burr Type III (BrIII) and Burr Type XII (BrXII) — were adopted to evaluate changes in design flood events for a range of return periods (up to 100 years) across historical and projected scenarios. While other distribution could be used, such as the Generalized Extreme Value (GEV) distribution—a widely used and highly flexible distribution (Coles, 2001), recent studies suggest that the Burr family offers advantages in specific hydrological contexts (Zaghloul et al., 2020; Ballarin et al., 2022). For instance, the upper bound of the GEV distribution (in its Weibull form, when the shape parameter assumes negative values) can constrain projections of physically unbounded flood magnitudes, especially for long return periods. In contrast, Burr distributions have no upper bound and include two shape parameters, allowing independent control over lower and upper tail heaviness.

The flexibility improves Burr distributions robustness in capturing complex tail behavior, a critical aspect in the assessment of extreme flood events (Papalexiou and Koutsoyiannis, 2012). Moreover, Burr distributions exhibit asymptotic behavior comparable to that of the GEV but avoid theoretical assumptions — such as block maxima drawn from an infinite sample — that are seldom met in practice. The distributions were fitted using the L-Moments method, and their suitability was evaluated through the L-Moments ratio diagram (Hosking, 1990; Vogel and Fennessey, 1993). For a detailed comparison of the strengths and limitations of the GEV, see Zaghloul et al. (2020).

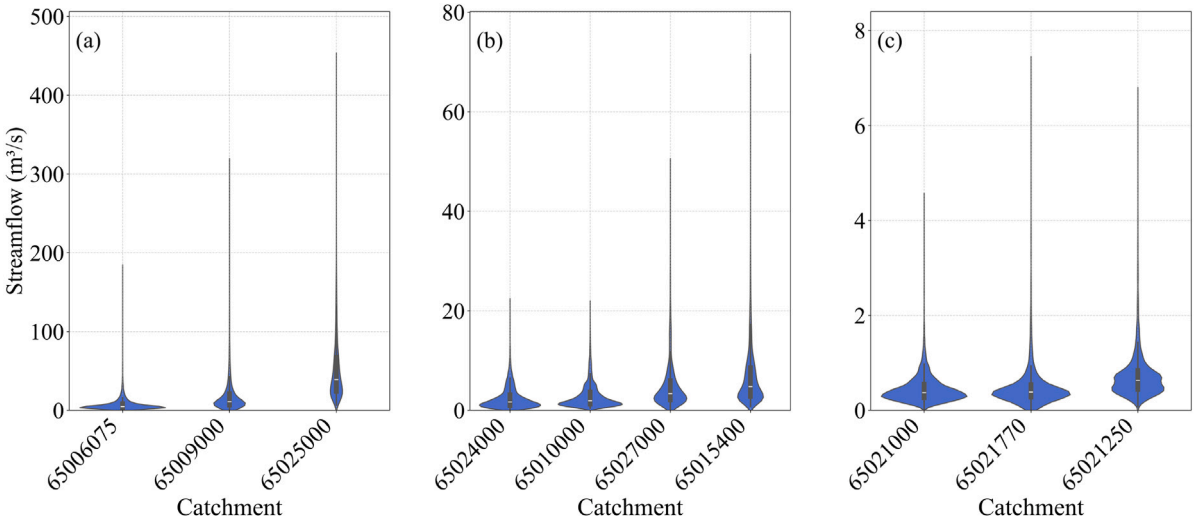

Fig. 4. Daily streamflow discharge variability across catchments during the 1986–2010 period. Catchments with higher (a), moderate (b), and lower (c) streamflow discharge. The Passaúna catchment is identified by code 65024000 in panel (b).

5. Results and discussion

5.1. Statistics of streamflow discharge

Although the ten catchments are geographically close (Fig. S1), their Q regimes differ markedly (Fig. 4). The first group of catchments exhibits highly variable Q, with median values ranging from 5 to 39 m^3/s (Fig. 4a). Catchments in this group present interquartile ranges from 3 to 67 m^3/s.

The second group demonstrates moderate variability, with median Q values between 2 and 5 m^3/s (Fig. 4b) and the interquartile range extends from 1 to 9 m^3/s (Fig. 4b) The third group displays more uniform Q distributions, with median values ranging from 0.4 to 0.6 m^3/s (Fig. 4c). Q values for this group range from 0.3 to 0.8 m^3/s based on interquartile statistics (Fig. 4c). Overall, across all catchments, the long-term mean monthly Q generally decreases from May to September and increases from October to March during the 1986–2010 observed period (Fig. S2).

5.2. Comparison between HyMod2 and LSTM

Fig. 5 presents a comparative assessment of observed and simulated Q, using HyMod2 and LSTM, for the Passaúna catchment. HyMod2 is considered the benchmark model. Additionally, based on the findings of Onyutha (2024), we take care to perform a fair comparison between the models by using KGE as the objective function. It is worth noting that LSTM was applied with k-fold = 1 (see Fig. 3) exclusively for comparison with HyMod2, as it shares the same validation period.

During the validation period, the HyMod2 exhibits agreement with observed data, effectively capturing overall daily Q dynamics (Fig. 5a), including rising and recession limbs, as indicated by high goodness-of-fit values ($KGE = 0.86$ and $NSE = 0.77$).

While both KGE and NSE indicate a high goodness-of-fit, they capture different aspects of the agreement between simulated and observed Q. The KGE combines correlation, bias, and variability components. In contrast, the NSE is more sensitive to peak-flows and large errors, particularly penalizing deviations during flood events. The $RMSE = 0.50$ mm/day indicates a reasonably low average error against observed Q.

Despite its satisfactory overall performance, HyMod2 performs poorly under extreme conditions, significantly underestimating drought flows ($FLV = -429.87\%$) and overestimating flood flows ($FHV = 38.80\%$). These results indicate systematic biases in simulating the lower 30% and upper 2% of the observed flow distribution, respectively (Fig. 5a). The HyMod2 parameters during calibration period are shown in Table S1.

LSTM model yields lower agreement with observed flows ($KGE = 0.75$ and $NSE = 0.64$) during the test period (Fig. 5b) compared to HyMod2. On the other hand, the $RMSE$ remains nearly unchanged at 0.63 mm/day. Notably, LSTM strongly overestimates flood flows ($FHV = 92.56\%$), while drought flows are better predicted ($FLV = 69.45\%$) than HyMod2, indicating a shift in behavior relative to HyMod2. This result suggests a reduction in underprediction during drought periods, albeit at the cost of amplifying flood flows.

Figure S3 presents the comparison between observed and simulated Q during the LSTM test period for each of the ten catchments. The LSTM model demonstrates generally good performance, with KGE values frequently approaching 0.70, except in two catchments (Fig. S3c,f), where performance was lower ($KGE \cong 0.40$). However, limitations are evident, particularly in the

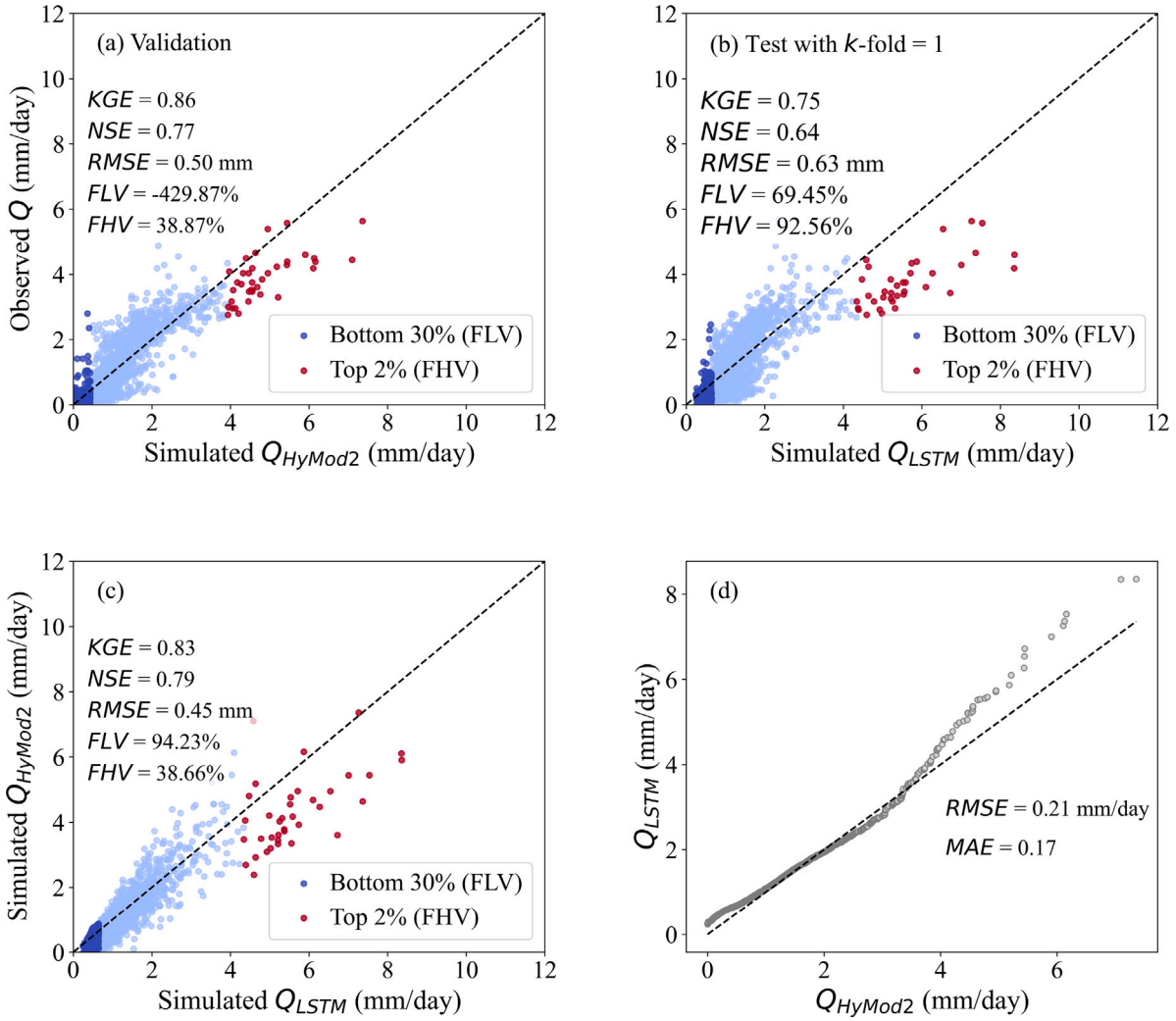

Fig. 5. Comparison between observed and simulated streamflow (Q) for the Passaúna catchment over the 2006–2010 period. (a) HyMod2 during the validation period. (b) LSTM during the test period (k-fold = 1). (c) Scatterplot comparing HyMod2 and LSTM Q outputs. HyMod2 is considered the benchmark model. (d) quantile–quantile plot. Q_{HyMod2} and Q_{LSTM} are the simulated streamflow by HyMod2 and LSTM, respectively, using observed data as input.

representation of low- and high-flow. The results indicate variability in LSTM performance across the catchments, suggesting that its sensitivity to local hydrological conditions may be influenced by the quality of the input data. This behavior can also be attributed to differences in physical and anthropogenic catchment characteristics, limitations in training data (e.g., short or biased records), and model configuration choices, all of which affect the ability to generalize and simulate extremes.

The comparison between the simulated Q of both models shows a high agreement (KGE = 0.83 and NSE = 0.79), with a relatively low $RMSE$ of 0.45 mm/day, indicating that both models produce broadly similar streamflow dynamics overall (Fig. 5c). Despite the strong overall agreement between HyMod2 and LSTM, the FLV = 94.23% and FHV = 38.66% reveal important differences in how each model simulates extreme flows (Fig. 5c). The high positive FLV value indicates that LSTM underestimates drought flows when compared to HyMod2, which may be attributed to HyMod2 representation of subsurface processes, such as soil moisture storage and groundwater contribution. Conversely, the FHV = 38.66% indicates that the LSTM overestimates flood flows relative to HyMod2 (Fig. 5c).

The quantile–quantile analysis (Fig. 5d) confirms close adherence between simulated and observed distributions ($RMSE$ = 0.21 mm/day and MAE = 0.17). The high agreement, especially in the middle part of the distribution, shows that both models generate similar Q values under overall flow dynamics. However, deviations occur at the lower and upper tails of the distribution, revealing persistent differences in how each model handles extreme flows (Fig. 5c,d).

5.3. Limitations in the models' performance

To be clear, similar results for dry and wet regimes (Fig. S4), as well as for drought (Fig. S5) and flood flows (Fig. S6), were obtained using outputs from both HyMod2 and LSTM. The comparison between these models reveals complementary strengths and limitations in simulating Q dynamics. While traditional performance metrics such as NSE and KGE indicate strong agreement, additional metrics like FHV and FLV — which focus on extreme flows — highlight persistent differences in their ability to simulate such conditions (Fig. 5c,d). HyMod2 demonstrated better performance in simulating flood flows, whereas LSTM exhibited simulation skill during drought conditions.

It is important to emphasize that the LSTM did not perform poorly; rather, it showed systematic deviations under extreme flow conditions. Although LSTMs have demonstrated potential in capturing overall characteristics such as long-term memory, nonlinearity, seasonality, and time lags in hydrological time series (Yang et al., 2019; Nearing et al., 2021), they may struggle to simulate extreme flows (Anwar et al., 2024) accurately. Some studies have demonstrated that pure LSTM models outperform a conceptual model, the Sacramento Model, in predicting peak flows (Frame et al., 2022).

Given the lack of consensus on this topic and contrasting performances on our modeling results, both LSTM and HyMod2 were used here to assess whether model structure significantly influences the projection of dry and wet regimes, including drought and flood flows, under future climate scenarios. The results for dry, wet, drought, and flood conditions presented hereafter were obtained using LSTM outputs based on k-fold = 5. This strategy was selected because it yielded the highest overall median KGE of 0.71, including the best individual performance ($KGE = 0.82$) for the Passaúna catchment (Table S2).

It is also worth noting that the LSTM model, implemented here as a single-layer neural network with a variable number of units, was easier to configure and train than the HyMod2, which requires extensive calibration and parameterization of physical processes. Consequently, this simplicity made LSTM more accessible in data-scarce environments, such as the ten catchments.

5.4. Future dry and wet regimes

The results of duration and severity indicate contrasting projected dynamics for dry and wet regimes in the Passaúna catchment (Fig. 6). Additional results for other accumulation intervals (3 and 12 months) (Fig. S7 and S8) and future periods (near and mid-century) (Fig. S9 and S10) are provided in the Supporting Material. No significant changes are projected for the dry regime regarding long-term drought duration and severity (Fig. 6a,b). For drought duration, there is considerable variability among CMIP6 simulations, mainly under the SSP5-8.5 scenario. In both scenarios, approximately half of the CMIP6 models project a reduction in drought duration. A similar pattern is observed for drought severity. Although the CMIP6 multi-model ensemble mean indicates slight increases under both scenarios, these changes are not statistically significant (Mann–Whitney U test, p-value = 0.05).

In contrast, the wet regime shows positive changes in both duration and severity, particularly under SSP5-8.5 (Fig. 6d,e). Despite the high inter-model variability, the multi-model mean projects increases of approximately 0.5 and 2 months in wet regime duration, and 10 and 33 mm in 6-month wet accumulation for SSP2-4.5 and SSP5-8.5, respectively. These results are consistent across accumulation intervals, indicating that both wet regime duration and severity are expected to increase in the far future for 3-, 6-, and 12-month accumulations. The contrasting trends between projected drought and wet conditions can be partially attributed to expected changes in monthly and annual Q (Fig. 6c,f). According to CMIP6 projections, monthly Q is expected to increase in the far future under both scenarios, particularly from April to December (Fig. 6c), leading to higher annual Q by the end of the century (Fig. 6f).

The results for both wet and dry regimes focus on projected changes in the long-term mean duration and severity. To further assess variability, the standard deviation of dry and wet regimes duration and severity was compared between historical and far future (Fig. S11 and S12). No significant changes are projected in the variability of drought duration and severity, indicating that future droughts are likely to retain statistical properties (mean and standard deviation) similar to those of the historical period. In contrast, wet regimes (Fig. S11 and S12) show substantial changes, particularly under the SSP5-8.5 scenario, with increases in both duration and severity. These findings suggest that future wet regimes in the Passaúna catchment may become more intense and variable, with a higher likelihood of extreme wet regime.

Notably, similar patterns of projected changes in dry and wet regimes were observed using Q simulated by the HyMod2 (Fig. S4). This consistency suggests that the choice of hydrological model does not substantially influence the projected changes, indicating that model structure is not the primary source of uncertainty. As supported by previous studies, the dominant source of uncertainty in climate change impact assessments on hydrology typically stems from climate simulations themselves (e.g., Chen et al., 2011; Her et al., 2019).

When evaluating dry and wet regimes from a meteorological rather than hydrological perspective — using P instead of Q — a marked increase in the severity of both regimes is evident (Fig. 7). However, no significant change is projected for the duration of dry regimes. This pattern may be attributed to the projected increase in water availability in southern Brazil, driven by expected rises in both moderate and extreme precipitation events (Ballarin et al., 2024b, 2023a). Nevertheless, these increases do not mitigate the severity of meteorological droughts due to shifts in the temporal distribution and seasonality of P, which are anticipated to intensify dry regimes even under higher overall rainfall (Ballarin et al., 2024a). Such intensification was likely not reflected in the hydrological analysis because of streamflow's memory effect, which buffers the influence of meteorological droughts through enhanced storage and delayed response.

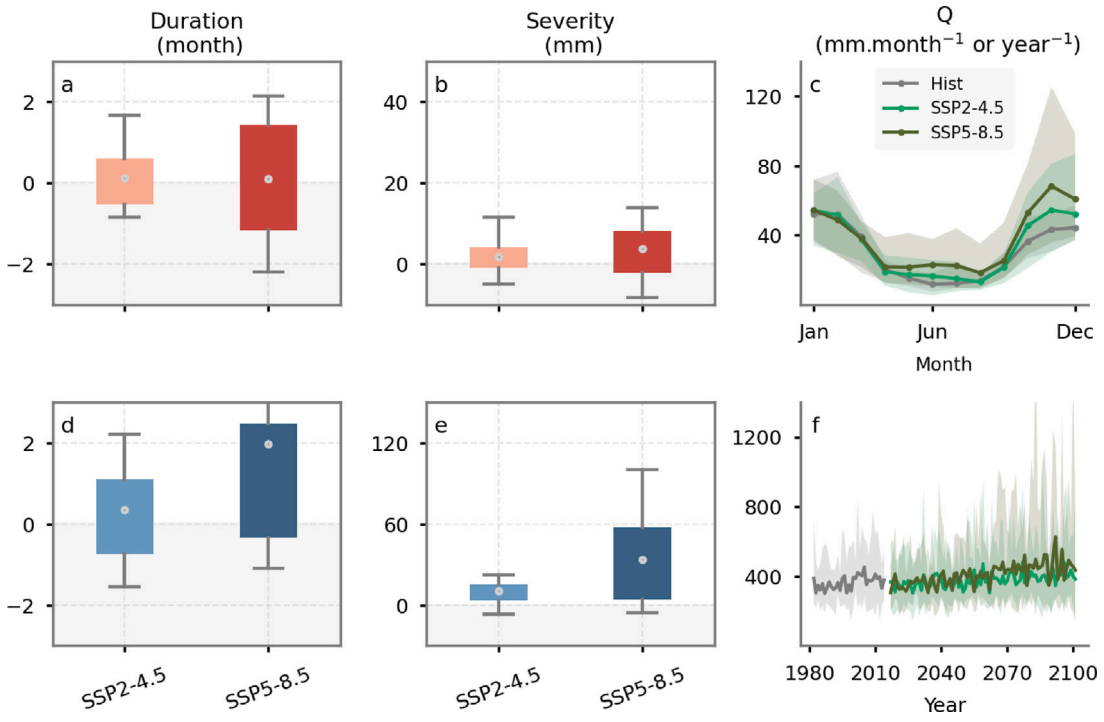

Fig. 6. Relative changes in the long-term mean duration and severity of dry (a, b) and wet (d, e) regimes between the historical and far future (2070–2100) periods under the SSP2-4.5 and SSP5-8.5 scenarios for the Passaúna catchment, based on a 6-month accumulation interval. Box plots show the CMIP6 multi-model spread, with the gray dot indicating the multi-model mean. Panels (c) and (f) display projected monthly and annual long-term streamflow (*Q*) under historical and SSP2-4.5 and SSP5-8.5 scenarios. Shaded areas represent the CMIP6 multi-model range (minimum to maximum), and solid lines correspond to the multi-model mean.

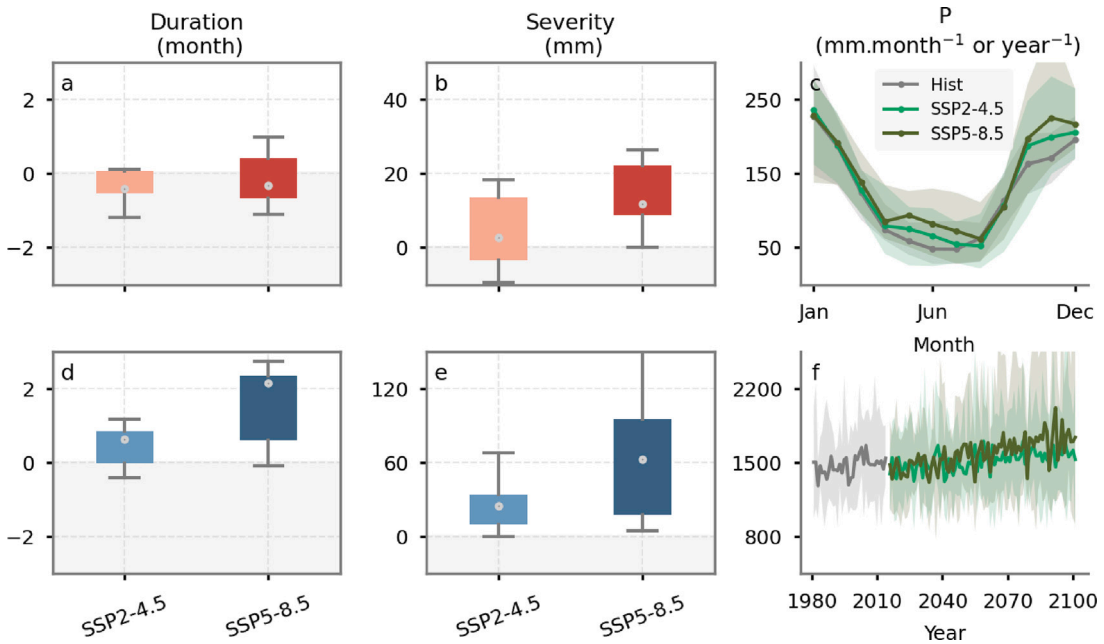

Fig. 7. Same as Fig. 6, but based on a meteorological perspective using precipitation (*P*) instead of streamflow (*Q*). Relative changes refer to the duration and severity of dry (a,b) and wet (d,e) periods derived from *P* data. Panels (c) and (f) show projected monthly and annual long-term *P* under historical and SSP2-4.5 and SSP5-8.5 scenarios. Box plots and shaded areas represent the CMIP6 multi-model ensemble.

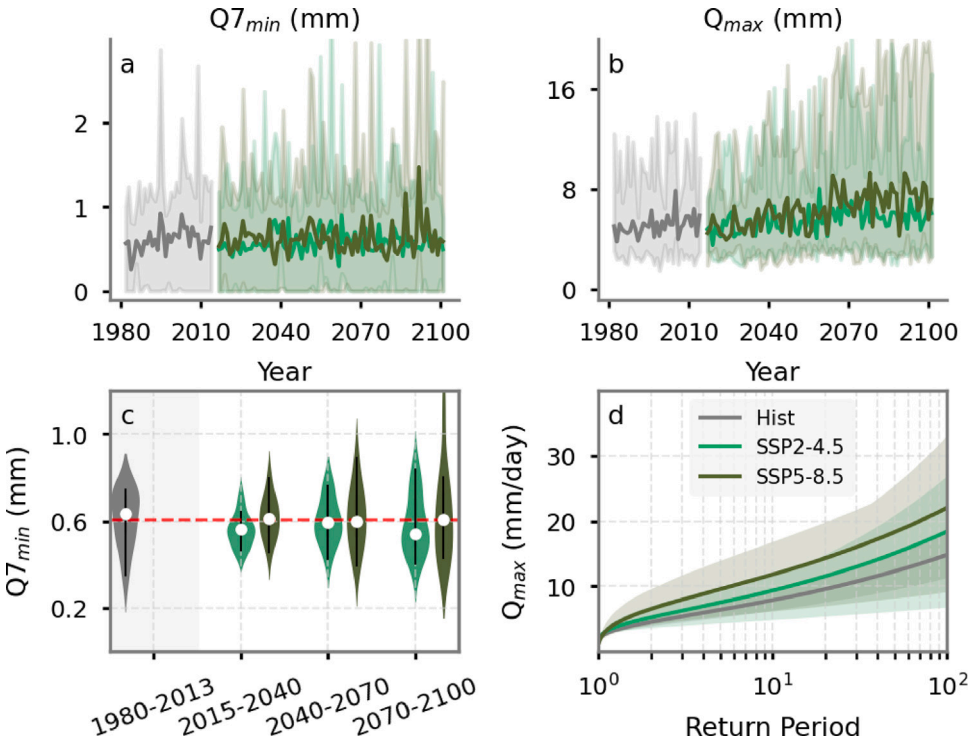

Fig. 8. Projected changes in future drought and flood flows. (a–b) Annual time series of $Q7_{min}$ and Q_{max} for the historical (1980–2013) and future (2015–2100) periods under the SSP2-4.5 and SSP5-8.5 scenarios. Shaded areas represent the CMIP6 multi-model spread (minimum to maximum), and solid lines show the multi-model mean. (c) Violin plots of $Q7_{min}$ for the near (2015–2040), middle (2040–2070), and far future (2070–2100) periods compared to the historical baseline. Each violin depicts the CMIP6 multi-model distribution; black lines indicate the interquartile range and white dots the median. The red dashed line denotes the historical multi-model mean. (d) Quantiles of Q_{max} estimated using the BrIII distribution for the historical and far future periods under SSP2-4.5 and SSP5-8.5. Shaded areas indicate the CMIP6 multi-model spread, and solid lines show the multi-model mean. (For interpretation of the references to color in this figure legend, the reader is referred to the web version of this article.)

5.5. Drought and flood flows

As expected from the preceding meteorological–hydrological analysis, projections for the Passaúna catchment indicate no substantial changes in drought flows but increased flood flows throughout the 21st century (Fig. 8). For drought flows ($Q7_{min}$), both SSP2-4.5 and SSP5-8.5 scenarios show no significant changes across all future periods (Mann–Kendall trend test, $p = 0.05$; Fig. 8c). These findings are consistent with earlier results indicating increased water availability and no significant shift in dry regimes (Fig. 6). In contrast, projections for flood flows (Q_{max}) indicate substantial increases, with a statistically significant upward trend observed under both scenarios (Mann–Kendall trend test, $p = 0.05$).

To further assess the implications of these changes in Q_{max} for hydraulic infrastructure design, the BrIII distribution were fitted — which outperformed BrXII based on L-moment ratio diagnostics (Fig. S13–S16) — to estimate design quantiles for return periods up to 100 years (Fig. 8d). For the far future, the 100-year design flood is projected to increase by approximately 26% under SSP2-4.5 and 52% under SSP5-8.5 relative to the historical period.

These projections align with previous studies that anticipate enhanced precipitation and extreme flooding in the region by century's end (e.g., Medeiros et al., 2022). For earlier future periods, changes are less pronounced: no significant increases are projected for the near future under either scenario (Fig. S17), while increases of 19% (SSP2-4.5) and 30% (SSP5-8.5) are projected for the middle future. Similar results were obtained using the traditional GEV distribution for simulated Q using the HyMod2, underscoring the robustness of the findings (Fig. S18). These results highlight a challenging future, particularly concerning intensified wet regimes and flood risk.

Besides assessing the suitability of the evaluated models using the L-Moments ratio diagram — a method widely used to test a set of probability distributions to describe extreme events or characterize sample properties (e.g., Peel et al., 2001; Salinas et al., 2014; Godoy et al., 2024; Zaerpour et al., 2024; Zaghloul et al., 2020) — the performance of the probability distribution models in terms of errors metrics, such as $RMSE$, MAE and goodness-of-fit test (Kolmogorov–Smirnov, KS, test) were also compared. These additional analyses supported our main conclusions. For instance, the GEV and BurrIII distributions obtained quite similar performance when applied to the historical bias-corrected simulations for all evaluated climate models (mean $RMSE$: GEV = 0.48 m^3/s; Burr Type III = 0.51 m^3/s; MAE: GEV = 0.29 m^3/s; Burr Type III = 0.30 m^3/s), and their suitability was confirmed by the KS test.

The choice to use the Burr Type III distribution is supported by the arguments presented in Papalexiou and Koutsoyiannis (2012) and Zaghloul et al. (2020). For instance, unlike the GEV distribution, which may have lower (or worse, upper) bounds depending on the shape parameter, the Burr Type III distribution is defined over the interval $(0, \infty)$, making it consistent with the potential range of streamflow values. It also has analytical expressions that are as simple as those of the GEV distribution, as well as a similar asymptotic behavior (i.e., it is a power-type distribution), making it suitable for modeling heavy tails. Furthermore, it is not a limiting extreme value distribution, and thus it does not require the assumption that maxima are extracted from an infinitely large sample, which clearly does not hold.

5.6. Limitations in extreme future scenarios

Although analyses point toward a wetter future in the Passaúna catchment, several caveats should be considered. First, climate model projections carry inherent uncertainties, particularly regarding the simulation of extreme events, which are often inadequately represented (Mishra et al., 2014; Sherwood et al., 2010). Indeed, climate models inherently carry uncertainties, not only due to their coarse spatial resolution — which limits their ability to capture local-scale climate processes — but also because they rely on parameterizations to represent complex or poorly understood physical processes. To address this, we adopted a widely accepted protocol involving bias correction and the use of a multi-model ensemble of CMIP6 projections (Addor et al., 2014; Muerth et al., 2013; Teutschbein and Seibert, 2012), which provides a range of plausible future climates. Nonetheless, bias-corrected datasets may still contain residual errors or unrealistic values (Casanueva et al., 2020; Santos et al., 2025).

Second, although machine learning models such as LSTM generally outperform traditional hydrological models in streamflow simulation (Kratzert et al., 2019a; Arsenault et al., 2023), they may struggle to capture extreme low- and high-flows due to their underrepresentation in training data. To assess uncertainty from the hydrological model structure, the analyses using HyMod2-derived streamflow series were carefully performed. Results remained consistent across both dry and wet regime analyses and in the projection of extremes, reinforcing the applicability of machine learning models for flood frequency analysis (Arsenault et al., 2023; Martel et al., 2024).

Finally, despite bias correction, substantial variability among CMIP6 models was observed, indicating that the choice of climate model inputs can significantly affect hydrological projections (Santos et al., 2025). Decision-makers should therefore account for this variability when designing adaptive measures. This variability reinforces findings from previous studies, which highlight climate model inputs as the dominant source of uncertainty in hydrological assessments under climate change (Chen et al., 2011; Her et al., 2019).

5.7. Implications to adaptive measures

This section presents the broader applicability of results and their relevance to regions facing similar climatic and hydrological challenges. Given the extended operational lifespans of dams, such as the Passaúna dam, evaluating climate change adaptation measures is essential (Bhaduri et al., 2016). Expanding storage capacity, increasing the number of dams, and adapting operational strategies may be necessary to mitigate vulnerabilities in water resource systems under projected climate scenarios (Ehsani et al., 2017).

In this context, results highlight a critical dynamics in hydrological regimes for the Passaúna catchment; while hydrological drought severity remains stable, flood risks are projected to increase significantly. It is important to emphasize that a non-significant increase in duration and severity in drought regime does not imply the absence of droughts, but rather indicates no significant change in their duration and or severity during the future period. In fact, recent droughts have posed significant challenges for water management in the Passaúna catchment. In this context, although evaporation losses were not the focus of this study, future adaptation strategies should also account for potential storage losses due to reservoir evaporation, even in temperate regions (e.g., Zhang et al., 2017).

The shifts in hydrometeorological patterns affect the design capacity and operational performance of dams, requiring adjustments to spillway management, flood storage allocation, and reservoir release policies to align with future hydrological conditions. As noted by Ehsani et al. (2017), water managers must balance competing priorities, such as maintaining reservoir storage for both flood and drought resilience while ensuring sufficient downstream water supply. Consequently, the Passaúna Dam's ability to mitigate floods and sustain water availability during dry regimes will be increasingly challenged.

The findings suggest that the 100-year flood event could increase by nearly 52% under the SSP5-8.5 scenario, posing significant challenges to adaptation measures. For instance, the effectiveness of reservoir operation as a potential adaptation strategy to mitigate climate change impacts should be addressed in future studies. However, previous studies have shown that relying solely on reservoir operation as an adaptation strategy under climate change will be insufficient to manage future floods, underscoring the need for complementary measures (Padiyedath Gopalan et al., 2021). Therefore, other adaptation measures for the Passaúna catchment may be considered, such as enhancing floodplain zoning through Payment for Environmental Services (PES). In Brazil, Payment for Ecosystem Services (PES) programs have well-defined objectives, primarily focused on water-related services. The most common goals include enhancing water discharge (91.25%) and improving water quality (85.00%). Additionally, many programs aim to promote vegetation growth (43.75%) and reduce sediment loads (36.25%), while a smaller proportion (21.25%) also targets socioeconomic benefits (Mamedes et al., 2023). The recovery of Passaúna catchment vegetation, particularly around river springs, dams, and flood-prone croplands, could be a key component of vegetation growth promotion.

As flood risks increase, croplands and natural vegetation in flood-prone areas of the Passaúna catchment are likely to face greater vulnerability, leading to significant crop loss, soil degradation, and disruption of local food production systems. Furthermore, increased flooding may elevate tree mortality due to prolonged inundation of floodplains, potentially disrupting moisture recycling and altering local and regional hydrological processes (Staal et al., 2018). Brazil is among the top ten countries with the highest cropland exposure to flooding (Zhang et al., 2023). To mitigate these risks, a combination of structural and non-structural strategies is essential. Physical measures such as flood walls and river training structures can protect croplands from inundation, while afforestation in upstream areas can reduce runoff and enhance water retention. Additionally, financial instruments like flood insurance provide a safety net for affected farmers, facilitating faster recovery from flood events. Integrating nature-based solutions, such as wetland restoration and green infrastructure, can further strengthen flood resilience while delivering co-benefits for biodiversity and water quality. Implementing these measures in the Passaúna catchment could enhance agricultural sustainability and reduce long-term flood impacts.

Another innovative approach to flood management is the concept of Flood Drainage Rights (FDR), a governance framework that establishes legal rights and responsibilities for regions to drain floodwaters into river reaches (Zhang et al., 2022). FDR ensures equitable and efficient floodwater management by balancing upstream and downstream needs during flood events. In the Yellow River Watershed in China, for example, FDR has been implemented to allocate flood drainage responsibilities among provinces based on hydrological capacity and historical flood patterns (Zhang et al., 2022). Under this system, upstream regions must manage excess water within predetermined quotas, preventing downstream flooding and minimizing economic and environmental damages. A similar framework could benefit the Passaúna catchment, where increasing flood frequency and intensity pose growing challenges for water managers. By defining clear floodwater management responsibilities between upstream and downstream areas, an FDR-based approach could enhance coordination among stakeholders, reduce flood damage, and improve resilience.

6. Conclusion

This study presents a comprehensive assessment of climate change impacts on hydrological regimes in the Passaúna catchment, a critical water source for the Curitiba Metropolitan Region, Brazil. Both LSTM and HyMod2 rainfall–runoff models demonstrated agreement with observed streamflow patterns, with low average errors indicating reliable performance under average flow conditions. However, limitations were identified in the simulation of extreme events: HyMod2 performed better for flood flows, whereas LSTM exhibited superior skill in capturing drought flows. Nevertheless, wet and dry regimes, as well as drought and flood flows, did not exhibit significant sensitivity to model structure.

Thus, the results of models' performance highlight the need for improved model representation of hydrological extremes. Some limitations might be attributed to the scarcity of ground-based observations in the study area. Consequently, we relied on global remote sensing-based products. While these datasets provide extensive spatial and temporal coverage, they also introduce uncertainties, especially under extreme hydroclimatic conditions.

Main findings indicate that the projections reveal contrasting shifts between dry and wet regimes. That is, no significant changes in dry regime under future climate scenarios and increased wet regime. While drought flows duration and severity are not expected to undergo substantial changes under future climate scenarios, the severity and duration of flood flows are projected to increase, particularly under SSP5-8.5 toward the end of the century. For example, the 100-year design flood is projected to increase by up to 52% under SSP5-8.5. Such trends are consistent across time scales, statistical methods, and hydrological modeling frameworks, reinforcing the robustness of flood hazard projections.

Despite the robustness of the methodological approach — including multi-model ensembles, bias correction, and the comparison of two structurally distinct hydrological models — uncertainties persist. These are primarily associated with the variability inherent in climate projections and, to a lesser extent, with differences in model performance for hydrological extremes. The results provide actionable insights for decision-makers, such as the Paraná Sanitation Company, as the projected increase in flood magnitudes underscores the importance of adaptive reservoir management and infrastructure resilience planning.

CRediT authorship contribution statement

Tiago Souza Mattos: Writing – review & editing, Visualization, Validation, Software, Methodology, Investigation, Formal analysis, Data curation, Conceptualization. **André Simões Ballarin:** Writing – original draft, Visualization, Validation, Software, Methodology, Investigation, Formal analysis, Data curation. **Murilo Cesar Lucas:** Writing – original draft, Visualization, Validation, Supervision, Resources, Project administration, Methodology, Investigation, Funding acquisition, Formal analysis, Conceptualization. **André Almagro:** Visualization, Software, Investigation. **Paulo Tarso Sanches Oliveira:** Writing – review & editing, Validation, Methodology, Investigation.

Declaration of competing interest

The authors declare the following financial interests/personal relationships which may be considered as potential competing interests: Murilo Cesar Lucas reports was provided by National Council for Scientific and Technological Development. If there are other authors, they declare that they have no known competing financial interests or personal relationships that could have appeared to influence the work reported in this paper.

Acknowledgments

MCL acknowledges the financial support from the National Council for Scientific and Technological Development—CNPq (403292/2023-9 Grant) and the Teaching, Research and Extension Support Fund – FAEPEX – of Unicamp (3111/23 Grant) .

Appendix A. Supplementary data

Supplementary material related to this article can be found online at https://doi.org/10.1016/j.ejrh.2025.102498.

Data availability

All data is available via open access repository at https://doi.org/10.7910/DVN/1C9NV2

Uneven shifts in flood and drought flows in a Brazilian water supply catchment - Dataset (Original data) (Havard Dataverse)

References

Addor, N., Rössler, O., Köplin, N., Huss, M., Weingartner, R., Seibert, J., 2014. Robust changes and sources of uncertainty in the projected hydrological regimes of swiss catchments. Water Resour. Res. 50 (10), 7541–7562. http://dx.doi.org/10.1002/2014WR015549, arXiv:https://agupubs.onlinelibrary.wiley.com/doi/pdf/10.1002/2014WR015549, URL: https://agupubs.onlinelibrary.wiley.com/doi/abs/10.1002/2014WR015549.

Alvares, C.A., Stape, J.L., Sentelhas, P.C., de Moraes Gonçalves, J.L., Sparovek, G., 2013. Köppen's climate classification map for Brazil. Meteorol. Z. 22 (6), 711–728. http://dx.doi.org/10.1127/0941?2948/2013/0507.

Anwar, H., Khan, A.U., Ullah, B., Taha, A.T.B., Najeh, T., Badshah, M.U., Ghanim, A.A.J., Irfan, M., 2024. Intercomparison of deep learning models in predicting streamflow patterns: insight from CMIP6. Sci. Rep. 14, 17468. http://dx.doi.org/10.1038/s41598-024-63989-7.

Arsenault, R., Martel, J.-L., Brunet, F., Brissette, F., Mai, J., 2023. Continuous streamflow prediction in ungauged basins: long short-term memory neural networks clearly outperform traditional hydrological models. Hydrol. Earth Syst. Sci. 27 (1), 139–157. http://dx.doi.org/10.5194/hess-27-139-2023, URL: https://hess.copernicus.org/articles/27/139/2023/.

Asadieh, B., Krakauer, N.Y., 2017. Global change in streamflow extremes under climate change over the 21st century. Hydrol. Earth Syst. Sci. 21 (11), 5863–5874. http://dx.doi.org/10.5194/hess-21-5863-2017, URL: https://hess.copernicus.org/articles/21/5863/2017/.

Ballarin, A.S., Calixto, K.G., Anache, J.A.A., Wendland, E., 2022. Combined predictive and descriptive tests for extreme rainfall probability distribution selection. Hydrol. Sci. J. http://dx.doi.org/10.1080/02626667.2022.2063725.

Ballarin, A.S., Gescilam Sousa Mota Uchôa, J., dos Santos, M.S., Miranda, I.P., Gustavo da Silva, P.C., da Silva, G.J., Júnior, G., Wendland, E., Tarso Oliveira, P.S., 2023a. Brazilian water security threatened by climate change and human behavior. Water Resour. Res. 59, e2023WR034914. http://dx.doi.org/10.1029/2023WR034914.

Ballarin, A.S., Sone, J.S., Gesualdo, G.C., Schwamback, D., Reis, A., Almagro, A., Wendland, E.C., 2023b. CLIMBra - climate change dataset for Brazil. Sci. Data 10 (1), http://dx.doi.org/10.1038/s41597-023-01956-z, URL: https://www.nature.com/articles/s41597-023-01956-z.

Ballarin, A.S., Vargas Godoy, M.R., Zaerpour, M., Abdelmoaty, H.M., Hatami, S., Gavasso-Rita, Y.L., Wendland, E., Papalexiou, S.M., 2024a. Drought intensification in Brazilian catchments: implications for water and land management. Environ. Res. Lett. 19 (5), 054030. http://dx.doi.org/10.1088/1748-9326/ad3e18.

Ballarin, A.S., Wendland, E., Zaerpour, M., Hatami, S., Neto, A.A.M., Papalexiou, S.M., 2024b. Frequency rather than intensity drives projected changes of rainfall events in Brazil. Earth' s Futur. 12, e2023EF004053. http://dx.doi.org/10.1029/2023EF004053, URL: https://onlinelibrary.wiley.com/doi/full/10.1029/2023EF004053 https://onlinelibrary.wiley.com/doi/abs/10.1029/2023EF004053 https://agupubs.onlinelibrary.wiley.com/doi/10.1029/2023EF004053.

Bartiko, D., Chaffe, P.L.B., Bonumá, N.B., 2017. Nonstationarity in maximum annual daily streamflow series from southern Brazil. RBRH 22, e48. http://dx.doi.org/10.1590/2318-0331.0217170054.

Beck, H.E., Wood, E.F., Pan, M., Fisher, C.K., Miralles, D.G., van Dijk, A.I.J.M., McVicar, T.R., Adler, R.F., 2019. MSWEP V2 global 3-hourly 0.1° precipitation: Methodology and quantitative assessment. Bull. Am. Meteorol. Soc. 100 (3), 473–500. http://dx.doi.org/10.1175/BAMS-D-17-0138.1, URL: https://journals.ametsoc.org/view/journals/bams/100/3/bams-d-17-0138.1.xml.

Bhaduri, A., Bogardi, J., Siddiqi, A., Voigt, H., Vörösmarty, C., Pahl-Wostl, C., Bunn, S.E., Shrivastava, P., Lawford, R., Foster, S., Kremer, H., Renaud, F.G., Bruns, A., Osuna, V.R., 2016. Achieving sustainable development goals from a water perspective. Front. Environ. Sci. 4, http://dx.doi.org/10.3389/fenvs.2016.00064, URL: https://www.frontiersin.org/journals/environmental-science/articles/10.3389/fenvs.2016.00064.

Boyle, D., 2001. Multicriteria Calibration of Hydrologic Models (Ph.D. thesis). The University of Arizona.

Brunner, M.I., Melsen, L.A., Newman, A.J., Wood, A.W., Clark, M.P., 2020. Future streamflow regime changes in the United States: assessment using functional classification. Hydrol. Earth Syst. Sci. 24 (8), 3951–3966. http://dx.doi.org/10.5194/hess-24-3951-2020, URL: https://hess.copernicus.org/articles/24/3951/2020/.

Cannon, A.J., Sobie, S.R., Murdock, T.Q., 2015. Bias correction of GCM precipitation by quantile mapping: How well do methods preserve changes in quantiles and extremes? J. Clim. 28 (17), 6938–6959. http://dx.doi.org/10.1175/JCLI-D-14-00754.1, URL: https://journals.ametsoc.org/view/journals/clim/28/17/jcli-d-14-00754.1.xml.

Casanueva, A., Herrera, S., Iturbide, M., Lange, S., Jury, M., Dosio, A., Maraun, D., Gutiérrez, J.M., 2020. Testing bias adjustment methods for regional climate change applications under observational uncertainty and resolution mismatch. Atmos. Sci. Lett. 21 (7), 1–12. http://dx.doi.org/10.1002/asl.978.

Chagas, V.B.P., Chaffe, P.L.B., Addor, N., Fan, F.M., Fleischmann, A.S., Paiva, R.C.D., Siqueira, V.A., 2020. CAMELS-BR: hydrometeorological time series and landscape attributes for 897 catchments in Brazil. Earth Syst. Sci. Data 12 (3), 2075–2096. http://dx.doi.org/10.5194/essd-12-2075-2020, URL: https://essd.copernicus.org/articles/12/2075/2020/ https://essd.copernicus.org/articles/12/2075/2020/essd-12-2075-2020.pdf.

Chagas, V.B.P., Chaffe, P.L.B., Blöschl, G., 2022. Climate and land management accelerate the Brazilian water cycle. Nat. Commun. 13, 5136. http://dx.doi.org/10.1038/s41467-022-32580-x.

Chen, J., Brissette, F.P., Poulin, A., Leconte, R., 2011. Overall uncertainty study of the hydrological impacts of climate change for a Canadian watershed. Water Resour. Res. 47 (12), http://dx.doi.org/10.1029/2011WR010602, arXiv:https://agupubs.onlinelibrary.wiley.com/doi/pdf/10.1029/2011WR010602, URL: https://agupubs.onlinelibrary.wiley.com/doi/abs/10.1029/2011WR010602.

Coles, S., 2001. An Introduction to Statistical Modeling of Extreme Values. Springer London, London, http://dx.doi.org/10.1007/978-1-4471-3675-0, URL: http://link.springer.com/10.1007/978-1-4471-3675-0.

Ehsani, N., Vörösmarty, C.J., Fekete, B.M., Stakhiv, E.Z., 2017. Reservoir operations under climate change: Storage capacity options to mitigate risk. J. Hydrol. 555, 435–446. http://dx.doi.org/10.1016/j.jhydrol.2017.09.008, URL: https://www.sciencedirect.com/science/article/pii/S0022169417305991.

Ficklin, D.L., Null, S.E., Abatzoglou, J.T., Novick, K.A., Myers, D.T., 2022. Hydrological intensification will increase the complexity of water resource management. Earth' s Futur. 10 (3), e2021EF002487. http://dx.doi.org/10.1029/2021EF002487, arXiv:https://agupubs.onlinelibrary.wiley.com/doi/pdf/10.1029/2021EF002487, URL: https://agupubs.onlinelibrary.wiley.com/doi/abs/10.1029/2021EF002487, e2021EF002487 2021EF002487.

Foufoula-Georgiou, E., Takbiri, Z., Czuba, J.A., Schwenk, J., 2015. The change of nature and the nature of change in agricultural landscapes: Hydrologic regime shifts modulate ecological transitions. Water Resour. Res. 51 (8), 6649–6671. http://dx.doi.org/10.1002/2015WR017637, arXiv:https://agupubs.onlinelibrary.wiley.com/doi/pdf/10.1002/2015WR017637, URL: https://agupubs.onlinelibrary.wiley.com/doi/abs/10.1002/2015WR017637.

Frame, J.M., Kratzert, F., Klotz, D., Gauch, M., Shalev, G., Gilon, O., Qualls, L.M., Gupta, H.V., Nearing, G.S., 2022. Deep learning rainfall–runoff predictions of extreme events. Hydrol. Earth Syst. Sci. 26 (13), 3377–3392. http://dx.doi.org/10.5194/hess-26-3377-2022, URL: https://hess.copernicus.org/articles/26/3377/2022/.

Gesualdo, G.C., Oliveira, P.T., Rodrigues, D.B.B., Gupta, H.V., 2019. Assessing water security in the são paulo metropolitan region under projected climate change. Hydrol. Earth Syst. Sci. 23, 4955–4968. http://dx.doi.org/10.5194/hess-23-4955-2019, URL: https://www.hydrol-earth-syst-sci.net/23/4955/2019/.

Godoy, M.R.V., Papalexiou, S.M., Markonis, Y., 2024. HYADES - a global archive of annual maxima daily precipitation. Sci. Data 11, 298. http://dx.doi.org/10.1038/s41597-024-03109-2.

Goodfellow, I., Bengio, Y., Courville, A., 2016. Deep Learning. MIT Press, http://www.deeplearningbook.org.

Gudmundsson, L., Boulange, J., Do, H.X., Gosling, S.N., Grillakis, M.G., Koutroulis, A.G., Leonard, M., Liu, J., Schmied, H.M., Papadimitriou, L., Pokhrel, Y., Seneviratne, S.I., Satoh, Y., Thiery, W., Westra, S., Zhang, X., Zhao, F., 2021. Globally observed trends in mean and extreme river flow attributed to climate change. Science 371 (6534), 1159–1162. http://dx.doi.org/10.1126/science.aba3996, arXiv:https://www.science.org/doi/pdf/10.1126/science.aba3996, URL: https://www.science.org/doi/abs/10.1126/science.aba3996.

Gupta, H.V., Kling, H., Yilmaz, K.K., Martinez, G.F., 2009. Decomposition of the mean squared error and NSE performance criteria: Implications for improving hydrological modelling. J. Hydrol. 377 (1–2), 80–91. http://dx.doi.org/10.1016/j.jhydrol.2009.08.003.

Her, Y., Yoo, S.-H., Cho, J., Hwang, S., Jeong, J., Seong, C., 2019. Uncertainty in hydrological analysis of climate change: multi-parameter vs. multi-GCM ensemble predictions. Sci. Rep. 9 (1), 4974.

Hilgert, S., Sotiri, K., Fuchs, S., 2019. Advanced assessment of sediment characteristics based on rheological and hydro-acoustic measurements in a Brazilian reservoir. Proc. IAHR World Congr. 61–70. http://dx.doi.org/10.3850/38WC092019-0616.

Hochreiter, S., Schmidhuber, J., 1997. Long short-term memory. Neural Comput. 9 (8), 1735–1780. http://dx.doi.org/10.1162/neco.1997.9.8.1735, arXiv:https://direct.mit.edu/neco/article-pdf/9/8/1735/813796/neco.1997.9.8.1735.pdf.

Hosking, J.R.M., 1990. L-moments: Analysis and estimation of distributions using linear combination of order statistics. J. R. Stat. Soc. 52 (1), 105–124. http://dx.doi.org/10.1111/j.2517-6161.1990.tb01775.x.

Koutsoyiannis, D., 2020. Revisiting the global hydrological cycle: is it intensifying? Hydrol. Earth Syst. Sci. 24 (8), 3899–3932. http://dx.doi.org/10.5194/hess-24-3899-2020, URL: https://hess.copernicus.org/articles/24/3899/2020/.

Kratzert, F., Gauch, M., Klotz, D., Nearing, G., 2024. HESS opinions: Never train an LSTM on a single basin. Hydrol. Earth Syst. Sci. Discuss. 2024, 1–19. http://dx.doi.org/10.5194/hess-2023-275, URL: https://hess.copernicus.org/preprints/hess-2023-275/.

Kratzert, F., Klotz, D., Brenner, C., Schulz, K., Herrnegger, M., 2018. Rainfall-runoff modelling using long short-term memory (LSTM) networks. Hydrol. Earth Syst. Sci. 22 (11), 6005–6022. http://dx.doi.org/10.5194/HESS-22-6005-2018.

Kratzert, F., Klotz, D., Herrnegger, M., Sampson, A.K., Hochreiter, S., Nearing, G.S., 2019a. Toward improved predictions in ungauged basins: Exploiting the power of machine learning. Water Resour. Res. 55 (12), 11344–11354. http://dx.doi.org/10.1029/2019WR026065, arXiv:https://agupubs.onlinelibrary.wiley.com/doi/pdf/10.1029/2019WR026065, URL: https://agupubs.onlinelibrary.wiley.com/doi/abs/10.1029/2019WR026065.

Kratzert, F., Klotz, D., Shalev, G., Klambauer, G., Hochreiter, S., Nearing, G., 2019b. Towards learning universal, regional, and local hydrological behaviors via machine learning applied to large-sample datasets. Hydrol. Earth Syst. Sci. 23 (12), 5089–5110. http://dx.doi.org/10.5194/hess-23-5089-2019, URL: https://hess.copernicus.org/articles/23/5089/2019/.

Liu, Y., Liu, F., Chen, C., Chen, Q., Zhang, J., Mo, K., Jiang, Q., Yao, S., 2024. A holistic approach to projecting streamflow and analyzing changes in ecologically relevant hydrological indicators under climate and land use/cover change. J. Hydrol. 632, 130863. http://dx.doi.org/10.1016/j.jhydrol.2024.130863, URL: https://www.sciencedirect.com/science/article/pii/S0022169424002579.

Mamedes, I., Guerra, A., Rodrigues, D.B., Garcia, L.C., Godoi, R.d., Oliveira, P.T.S., 2023. Brazilian payment for environmental services programs emphasize water-related services. Int. Soil Water Conserv. Res. 11 (2), 276–289. http://dx.doi.org/10.1016/j.iswcr.2023.01.001, URL: https://www.sciencedirect.com/science/article/pii/S2095633923000011.

Mapbiomas, 2023. Project MapBiomas - collection 7.0 of Brazilian land cover & use map series. URL: https://mapbiomas.org/.

Martel, J.-L., Arsenault, R., Turcotte, R., Castañeda-Gonzalez, M., Brissette, F., Armstrong, W., Mailhot, E., Pelletier-Dumont, J., Lachance-Cloutier, S., Rondeau-Genesse, G., Caron, L.-P., 2024. Exploring the ability of LSTM-based hydrological models to simulate streamflow time series for flood frequency analysis. EGUsphere 2024, 1–32. http://dx.doi.org/10.5194/egusphere-2024-2134, URL: https://egusphere.copernicus.org/preprints/2024/egusphere-2024-2134/.

Martens, B., Miralles, D.G., Lievens, H., van der Schalie, R., de Jeu, R.A.M., Fernández-Prieto, D., Beck, H.E., Dorigo, W.A., Verhoest, N.E.C., 2017. GLEAM v3: satellite-based land evaporation and root-zone soil moisture. Geosci. Model. Dev. 10 (5), 1903–1925. http://dx.doi.org/10.5194/gmd-10-1903-2017, URL: https://www.geosci-model-dev.net/10/1903/2017/.

Mckee, T.B., Doesken, N.J., Kleist, J., 1993. The relationship of drought frequency and duration to time scales. Eighth Conf. Appl. Clim. 17–22.

Medeiros, F.j., Oliveira, C.P., Avila-Diaz, A., 2022. Evaluation of extreme precipitation climate indices and their projected changes for Brazil: From CMIP3 to CMIP6. Weather. Clim. Extrem. 38, 100511. http://dx.doi.org/10.1016/j.wace.2022.100511, Publisher: Elsevier B.V..

Meira Neto, A.A., Medeiros, P., de Araújo, J.C., Pereira, B., Sivapalan, M., 2024. Evolution of drought mitigation and water security through 100 years of reservoir expansion in semi-arid Brazil. Water Resour. Res. 60 (9), e2023WR036411. http://dx.doi.org/10.1029/2023WR036411, arXiv:https://agupubs.onlinelibrary.wiley.com/doi/pdf/10.1029/2023WR036411, URL: https://agupubs.onlinelibrary.wiley.com/doi/abs/10.1029/2023WR036411, e2023WR036411 2023WR036411.

Melo, D.d.C.D., Scanlon, B.R., Zhang, Z., Wendland, E., Yin, L., 2016. Reservoir storage and hydrologic responses to droughts in the paraná river basin, southeastern Brazil. Hydrol. Earth Syst. Sci. 20 (11), 4673–4688. http://dx.doi.org/10.5194/hess-20-4673-2016, URL: https://www.hydrol-earth-syst-sci.net/20/4673/2016/.

Milly, P.C.D., Betancourt, J., Falkenmark, M., Hirsch, R.M., Kundzewicz, Z.W., Lettenmaier, D.P., Stouffer, R.J., 2008. Stationarity is dead: Whither water management? Science 319, 573 LP – 574. http://dx.doi.org/10.1126/science.1151915, URL: http://science.sciencemag.org/content/319/5863/573.abstract.

Mishra, V., Kumar, D., Ganguly, A.R., Sanjay, J., Mujumdar, M., Krishnan, R., Shah, R.D., 2014. Reliability of regional and global climate models to simulate precipitation extremes over India. J. Geophys. Res.: Atmos. 119, 9301–9323. http://dx.doi.org/10.1002/2014JD021636.

Muerth, M.J., Gauvin St-Denis, B., Ricard, S., Velázquez, J.A., Schmid, J., Minville, M., Caya, D., Chaumont, D., Ludwig, R., Turcotte, R., 2013. On the need for bias correction in regional climate scenarios to assess climate change impacts on river runoff. Hydrol. Earth Syst. Sci. 17 (3), 1189–1204. http://dx.doi.org/10.5194/hess-17-1189-2013, URL: https://hess.copernicus.org/articles/17/1189/2013/.

Nash, J.E., Sutcliffe, J.V., 1970. River flow forecasting through conceptual models part I — A discussion of principles. J. Hydrol. 10, 282–290. http://dx.doi.org/10.1016/0022-1694(70)90255-6.

Nearing, G.S., Kratzert, F., Sampson, A.K., Pelissier, C.S., Klotz, D., Frame, J.M., Prieto, C., Gupta, H.V., 2021. What role does hydrological science play in the age of machine learning? Water Resour. Res. 57 (3), e2020WR028091. http://dx.doi.org/10.1029/2020WR028091, arXiv:https://agupubs.onlinelibrary.wiley.com/doi/pdf/10.1029/2020WR028091, URL: https://agupubs.onlinelibrary.wiley.com/doi/abs/10.1029/2020WR028091, e2020WR028091 10.1029/2020WR028091.

O'Neill, B.C., Tebaldi, C., van Vuuren, D.P., Eyring, V., Friedlingstein, P., Hurtt, G., Knutti, R., Kriegler, E., Lamarque, J.-F., Lowe, J., Meehl, G.A., Moss, R., Riahi, K., Sanderson, B.M., 2016. The scenario model intercomparison project (ScenarioMIP) for CMIP6. Geosci. Model. Dev. 9 (9), 3461–3482. http://dx.doi.org/10.5194/gmd-9-3461-2016, URL: https://gmd.copernicus.org/articles/9/3461/2016/.

Onyutha, C., 2024. Pros and cons of various efficiency criteria for hydrological model performance evaluation. Proc. IAHS 385, 181–187. http://dx.doi.org/10.5194/piahs-385-181-2024, URL: https://piahs.copernicus.org/articles/385/181/2024/.

Orth, R., Seneviratne, S.I., 2012. Analysis of soil moisture memory from observations in Europe. J. Geophys. Res.: Atmos. 117 (D15), http://dx.doi.org/10.1029/2011JD017366, arXiv:https://agupubs.onlinelibrary.wiley.com/doi/pdf/10.1029/2011JD017366, URL: https://agupubs.onlinelibrary.wiley.com/doi/abs/10.1029/2011JD017366.

Padiyedath Gopalan, S., Hanasaki, N., Champathong, A., Tebakari, T., 2021. Impact assessment of reservoir operation in the context of climate change adaptation in the chao phraya river basin. Hydrol. Process. 35 (1), e14005. http://dx.doi.org/10.1002/hyp.14005, arXiv:https://onlinelibrary.wiley.com/doi/pdf/10.1002/hyp.14005, URL: https://onlinelibrary.wiley.com/doi/abs/10.1002/hyp.14005.

Papalexiou, S.M., Koutsoyiannis, D., 2012. Entropy based derivation of probability distributions: A case study to daily rainfall. Adv. Water Resour. 45, 51–57. http://dx.doi.org/10.1016/j.advwatres.2011.11.007, URL: https://linkinghub.elsevier.com/retrieve/pii/S0309170811002193.

Peel, M.C., Wang, Q.J., Vogel, R.M., And, T.A.M., 2001. The utility of L-moment ratio diagrams for selecting a regional probability distribution. Hydrol. Sci. J. 46 (1), 147–155. http://dx.doi.org/10.1080/02626660109492806.

Rezvani, R., RahimiMovaghar, M., Na, W., Najafi, M.R., 2023. Hydrological changes under 1.5°C – 4°C global warming levels. J. Hydrol. 624, 129906. http://dx.doi.org/10.1016/j.jhydrol.2023.129906, URL: https://www.sciencedirect.com/science/article/pii/S002216942300848X.

Roy, T., Gupta, H.V., Serrat-Capdevila, A., Valdes, J.B., 2017. Using satellite-based evapotranspiration estimates to improve the structure of a simple conceptual rainfall-runoff model. Hydrol. Earth Syst. Sci. 21 (2), 879–896. http://dx.doi.org/10.5194/HESS-21-879-2017.

Salinas, J.L., Castellarin, A., Kohnová, S., Kjeldsen, T.R., 2014. Regional parent flood frequency distributions in europe – part 2: Climate and scale controls. Hydrol. Earth Syst. Sci. 18 (11), 4391–4401. http://dx.doi.org/10.5194/hess-18-4391-2014, URL: https://hess.copernicus.org/articles/18/4391/2014/.

Santos, L.R., Barbosa, A.d., Leite, C.C.O., Silva, G.M.e., Mendiondo, E.M., Costa, V.A.F., 2025. Assessing future changes in hydroclimatic processes in the Metropolitan Region of Belo Horizonte, Brazil, with the expanded Bluecat framework. Front. Water 7, 1541052.

Satgé, F., Pillot, B., Roig, H., Bonnet, M.-P., 2021. Are gridded precipitation datasets a good option for streamflow simulation across the Juruá river basin, Amazon? J. Hydrol. 602, 126773. http://dx.doi.org/10.1016/j.jhydrol.2021.126773, URL: https://www.sciencedirect.com/science/article/pii/S0022169421008234.

Satoh, Y., Yoshimura, K., Pokhrel, Y., Kim, H., Shiogama, H., Yokohata, T., Hanasaki, N., Wada, Y., Burek, P., Byers, E., Schmied, H.M., Gerten, D., Ostberg, S., Gosling, S.N., Boulange, J.E.S., Oki, T., 2022. The timing of unprecedented hydrological drought under climate change. Nat. Commun. 13, 3287. http://dx.doi.org/10.1038/s41467-022-30729-2.

Scanlon, B.R., Fakhreddine, S., Rateb, A., de Graaf, I., Famiglietti, J., Gleeson, T., Grafton, R.Q., Jobbagy, E., Kebede, S., Kolusu, S.R., Konikow, L.F., Long, D., Mekonnen, M., Schmied, H.M., Mukherjee, A., MacDonald, A., Reedy, R.C., Shamsudduha, M., Simmons, C.T., Sun, A., Taylor, R.G., Villholth, K.G., Vörösmarty, C.J., Zheng, C., 2023. Global water resources and the role of groundwater in a resilient water future. Nat. Rev. Earth Environ. 2023 1–15. http://dx.doi.org/10.1038/s43017-022-00378-6, URL: https://www.nature.com/articles/s43017-022-00378-6.

Sherwood, S.C., Roca, R., Weckwerth, T.M., Andronova, N.G., 2010. Tropospheric water vapor, convection, and climate. Rev. Geophys. 48 (2), 1–29. http://dx.doi.org/10.1029/2009RG000301.

Staal, A., Tuinenburg, O.A., Bosmans, J.H.C., Holmgren, M., van Nes, E.H., Scheffer, M., Zemp, D.C., Dekker, S.C., 2018. Forest-rainfall cascades buffer against drought across the Amazon. Nat. Clim. Chang. 8, 539–543. http://dx.doi.org/10.1038/s41558-018-0177-y.

Tabari, H., 2020. Climate change impact on flood and extreme precipitation increases with water availability. Sci. Rep. 10, 13768. http://dx.doi.org/10.1038/s41598-020-70816-2, URL: https://doi.org/10.1038/s41598-020-70816-2.

Teutschbein, C., Seibert, J., 2012. Bias correction of regional climate model simulations for hydrological climate-change impact studies: Review and evaluation of different methods. J. Hydrol. 456–457, 12–29. http://dx.doi.org/10.1016/j.jhydrol.2012.05.052, URL: https://www.sciencedirect.com/science/article/pii/S0022169412004556.

Ukkola, A.M., De Kauwe, M.G., Roderick, M.L., Abramowitz, G., Pitman, A.J., 2020. Robust future changes in meteorological drought in CMIP6 projections despite uncertainty in precipitation. Geophys. Res. Lett. 47 (11), e2020GL087820. http://dx.doi.org/10.1029/2020GL087820, arXiv:https://agupubs.onlinelibrary.wiley.com/doi/pdf/10.1029/2020GL087820, URL: https://agupubs.onlinelibrary.wiley.com/doi/abs/10.1029/2020GL087820, e2020GL087820 2020GL087820.

United Nations, 2015. The Millennium Development Goals Report. United Nations, New York, p. 75.

Van Loon, A.F., Van Lanen, H.A., 2013. Making the distinction between water scarcity and drought using an observation-modeling framework. Water Resour. Res. 49 (3), 1483–1502. http://dx.doi.org/10.1002/wrcr.20147.

Vogel, R.M., Fennessey, N.M., 1993. *L* moment diagrams should replace product moment diagrams. Water Resour. Res. 29 (6), 1745–1752. http://dx.doi.org/10.1029/93WR00341, URL: https://agupubs.onlinelibrary.wiley.com/doi/10.1029/93WR00341.

Wagener, T., Boyle, D.P., Lees, M.J., Wheater, H.S., Gupta, H.V., Sorooshian, S., 2001. A framework for development and application of hydrological models. Hydrol. Earth Syst. Sci. 5, 13–26. http://dx.doi.org/10.5194/hess-5-13-2001.

Wang, Y., Meili, N., Fatichi, S., 2023. Evidence and controls of the acceleration of the hydrological cycle over land. Water Resour. Res. 59 (8), e2022WR033970. http://dx.doi.org/10.1029/2022WR033970, arXiv:https://agupubs.onlinelibrary.wiley.com/doi/pdf/10.1029/2022WR033970, URL: https://agupubs.onlinelibrary.wiley.com/doi/abs/10.1029/2022WR033970, e2022WR033970 2022WR033970.

Wang, T., Tu, X., Singh, V.P., Chen, X., Lin, K., 2021. Global data assessment and analysis of drought characteristics based on CMIP6. J. Hydrol. 596, 126091. http://dx.doi.org/10.1016/j.jhydrol.2021.126091, URL: https://www.sciencedirect.com/science/article/pii/S0022169421001384.

Wang, Y.-y., Wang, W.-c., Xu, D.-m., Zhao, Y.-w., Zang, H.-f., 2024. A compound approach for ten-day runoff prediction by coupling wavelet denoising, attention mechanism, and LSTM based on GPU parallel acceleration technology. Earth Sci. Inform. 17 (2), 1281–1299.

Xavier, A.C., King, C.W., Scanlon, B.R., 2016. Daily gridded meteorological variables in Brazil (1980–2013). Int. J. Climatol. 36 (6), 2644–2659. http://dx.doi.org/10.1002/joc.4518, arXiv:https://rmets.onlinelibrary.wiley.com/doi/pdf/10.1002/joc.4518, URL: https://rmets.onlinelibrary.wiley.com/doi/abs/10.1002/joc.4518.

Xu, D.-m., Liao, A.-d., Wang, W., Tian, W.-c., Zang, H.-f., 2023. Improved monthly runoff time series prediction using the CABES-LSTM mixture model based on CEEMDAN-VMD decomposition. J. Hydroinformatics 26 (1), 255–283. http://dx.doi.org/10.2166/hydro.2023.216, arXiv:https://iwaponline.com/jh/article-pdf/26/1/255/1361150/jh0260255.pdf.

Yang, Q., Zhang, H., Wang, G., Luo, S., Chen, D., Peng, W., Shao, J., 2019. Dynamic runoff simulation in a changing environment: A data stream approach. Environ. Model. Softw. 112, 157–165. http://dx.doi.org/10.1016/j.envsoft.2018.11.007, URL: https://www.sciencedirect.com/science/article/pii/S1364815218308351.

Yilmaz, K.K., Gupta, H.V., Wagener, T., 2008. A process-based diagnostic approach to model evaluation: Application to the NWS distributed hydrologic model. Water Resour. Res. 44, http://dx.doi.org/10.1029/2007WR006716.

Yu, T., Zhu, H., 2020. Hyper-parameter optimization: A review of algorithms and applications. arXiv:2003.05689, URL: https://arxiv.org/abs/2003.05689.

Zaerpour, M., Papalexiou, S.M., Pietroniro, A., Nazemi, A., 2024. How extreme are flood peak distributions? A quasi-global analysis of daily discharge records. J. Hydrol. 631, 130849. http://dx.doi.org/10.1016/j.jhydrol.2024.130849, URL: https://www.sciencedirect.com/science/article/pii/S0022169424002439.

Zaghloul, M., Papalexiou, S.M., Elshorbagy, A., Coulibaly, P., 2020. Revisiting flood peak distributions: A pan-Canadian investigation. Adv. Water Resour. 145, 103720. http://dx.doi.org/10.1016/j.advwatres.2020.103720, Publisher: Elsevier Ltd.

Zhang, K., Dong, Z., Guo, L., Boyer, E.W., Mello, C.R., Shen, J., Lan, P., Wang, J., Fan, B., 2022. Allocation of flood drainage rights in the middle and lower reaches of the yellow river based on deep learning and flood resilience. J. Hydrol. 615, 128560. http://dx.doi.org/10.1016/j.jhydrol.2022.128560, URL: https://www.sciencedirect.com/science/article/pii/S0022169422011301.

Zhang, H., Gorelick, S.M., Zimba, P.V., Zhang, X., 2017. A remote sensing method for estimating regional reservoir area and evaporative loss. J. Hydrol. 555, 213–227. http://dx.doi.org/10.1016/j.jhydrol.2017.10.007, URL: https://www.sciencedirect.com/science/article/pii/S0022169417306716.

Zhang, Y., Keenan, T.F., Zhou, S., 2021. Exacerbated drought impacts on global ecosystems due to structural overshoot. Nat. Ecol. Evol. 5, 1490–1498. http://dx.doi.org/10.1038/s41559-021-01551-8.

Zhang, M., Zhai, G., He, T., Wu, C., 2023. A growing global threat: Long-term trends show cropland exposure to flooding on the rise. Sci. Total Environ. 899, 165675. http://dx.doi.org/10.1016/j.scitotenv.2023.165675, URL: https://www.sciencedirect.com/science/article/pii/S0048969723042985.